

Noncommutative Schwarzschild black hole surrounded by quintessence: Thermodynamics, Shadows and Quasinormal modes

B. Hamil*

Laboratoire de Physique Mathématique et Subatomique,
Faculté des Sciences Exactes, Université Constantine 1, Constantine, Algeria.

B. C. Lütfüoğlu†

Department of Physics, University of Hradec Králové,
Rokitanského 62, 500 03 Hradec Králové, Czechia.

April 11, 2024

Abstract

In (Sci. Rep. **12**, 8516 (2022)), Campos et al studied the quasinormal modes and shadows of noncommutative Schwarzschild black holes. Since we know that the quintessence matter surrounding black holes has significant effects on the black hole quantities, in this study, we aimed to show this influence by revisiting the same problem in the presence of quintessence matter field. To this end, we first examined the thermodynamics of noncommutative Schwarzschild black holes embedded in quintessence matter using Hawking temperature, entropy, and specific heat functions. After that, we discussed phase transition and stability features. We then investigated the shadow images in the presence of plasma. After visualizing these results qualitatively, we calculated the quasinormal modes in WKB and Mashhoon approximations and we demonstrated the impacts of quintessence matter and noncommutative spacetime on the whole quantities.

1 Introduction

Before the nineteen seventies, there was no significant motivation to debate the black holes in the framework of their thermodynamics. This perspective changed drastically in 1973 with the remarkable paper of Bekenstein [1], in which the entropy of a black hole was related to the black hole's area via Hawking's theorem [2]. In the same year, Bardeen et al. employed an analogy between surface gravity and temperature in addition to the existing one between the entropy and event horizon surface area, so they stated four fundamental laws to investigate black hole thermodynamics [3]. Two years later, Hawking refuted the contradictory ideas of the classical approach that black holes should absorb all matter and energy without emitting radiation theoretically [4]. According to him, quantum effects had to play a critical role in black holes, thus, black holes could also emit radiation characterized by a spectrum similar to that of a black body with a specific temperature. In the following years, Hawking's

*hamilbilel@gmail.com, bilel.hamil@edu.umc.dz

†bekir.lutfuoglu@uhk.cz (Corresponding author)

interpretation was confirmed by many other independent ways [5], which led to an increase in studies discussing the thermal properties of black holes [6–18].

Distinguished observations in the last decade of the last century, based on the magnitude-redshift relation of astronomical objects, have revealed that the universe is expanding at an accelerating rate [19–21]. Since the theoretically predicted value of the cosmological constant, which is expected to correspond to this phenomenon in the general theory of relativity via the action,

$$\mathcal{S} = \frac{1}{16\pi G} \int d^4x \sqrt{-g} [R + 2\Lambda] + \mathcal{S}_{\mathcal{M}}, \quad (1)$$

differs from the observational value by 120 orders of magnitude [22], alternative explanations have begun to be considered. Some theorists thought that dark energy, distributed relatively uniformly in space with a negative pressure, could be responsible for this [23]. In the literature, dark energy is modeled by using dynamic scalar fields with different state parameter equations [24–30]. One of the most examined forms is given by the quintessence matter model with the action

$$\mathcal{S} = \int d^4x \sqrt{-g} \left[\frac{R}{16\pi G} + \mathcal{L}_{quin} \right] + \mathcal{S}_{\mathcal{M}}, \quad (2)$$

where the quintessence term is coupled to the action by the Lagrange density term

$$\mathcal{L}_{quin} = -\frac{1}{2} (\nabla\phi)^2 - V(\phi), \quad (3)$$

with the quintessential scalar field, ϕ , and potential, $V(\phi)$.

In this theory, the universe's dark energy is primarily dominated by the potential of the scalar field, which is continuously evolving towards its minimum at $V = 0$. Usually, this minimum is situated at $\phi = \infty$, and the scalar potential may have a form such as $V \sim e^{-c\phi}$. The theory can also be parameterized by an equation of state of the usual form [31, 32]

$$P = \omega_q \rho, \quad (4)$$

where P is the pressure and ρ is the energy density. In this approach, the equation of state parameter has to be in the range $-1 < \omega_q < -1/3$ [33]. In 2003, Kiselev derived a general form of the static spherically symmetric solutions of Einstein's equations and presented the line elements of electrically uncharged and charged black holes surrounded by quintessence matter [34]. Following this work, some other physicists obtained new solutions corresponding to various black holes of different properties in the presence of quintessence matter [35–47]. Recently, with the growing interest in black hole thermodynamics, we have observed a growing interest in the studies discussing the influence of quintessence matter on the thermal quantities of black holes [48–60].

Until recent years, one of the main concerns about black holes was about their observations. Even if they could not be observed directly, could their effects, that is, their fingerprints, be detected? One of the ideas in the ongoing debates in this direction was based on the argument that real black holes should not be an ideally isolated system. Accordingly, after the gravitational collapse of matter, black holes should be formed in a perturbed state, and thus their fundamental parameters, namely their masses, charges, and angular momenta should not be enough to discuss their features, i.e. stability, Hawking radiation... A perturbed black hole is assumed to oscillate the background by emitting gravitational waves, which are damped after a short while of the initial outburst of radiation over time. In the literature, these particular oscillation frequencies are called the quasinormal modes (QNMs) [61]. Mathematically, these modes appear in complex number forms, where their real parts denote the actual oscillation, while their complex parts correspond to the damping time inversely [62]. Interestingly, QNMs were found

to be independent of the initial perturbation, and thus, they are accepted as the fingerprints of black holes [63]. Following the great success of the LIGO-VIRGO collaboration in detecting gravitational waves [64, 65], interest in QNMs has increased enormously [66–95].

One of the other fingerprints of black holes is their shadows. Very recently, with joint work, Event Horizon Telescope succeeded in determining black hole shadows [96, 97]. This observation is based on detecting the photon deflections radiated by strong light sources in the background of the black holes [98]. According to the modeling, when light rays pass near a black hole, only photons with low orbital angular momentum are trapped and photons with high orbital angular momentum are deflected. Therefore, depending on the observing position, the observer observes dark regions in the observational sky [99]. Historically, the theoretical estimation of the concept of shadow dates back half a century [100–102], but it was only after the aforementioned observations that it began to be studied intensively [103–140].

The final stage of black hole evaporation is still debated in the literature. According to some views, string effects should be taken into account at this stage, and noncommutative geometry, which has a long history [141], could be a suitable approach to account for these extreme quantum gravitational effects [142]. From this point of view, in 2005 two independent studies, first Nicollini [143] and then Nasserri [144], considered Schwarzschild black holes in non-commutative geometry. The following year, Nicolini et al demonstrated that noncommutative effects vanish several problems in the evaporation process [145]. Then, Rizzo showed that in the presence of extra dimensions significant modifications emerge [146]. After these cornerstone studies, other black holes and their features have also been extensively investigated in noncommutative geometry [147–168]. Recently, in [169–173] authors examined the QNMs of the Schwarzschild-like black holes. Moreover, Campos et al derived the shadow radius and discussed the impact of the noncommutativity parameter on it in [173].

Inspired by all these facts, in this manuscript, we intend to determine the impact of the quintessence matter on the thermal quantities, stability, and phase transitions of the Schwarzschild black hole in noncommutative spacetime. Moreover, we aim to investigate the shadows and QNMs of the black hole and demonstrate the influence of the quintessence matter on them. To this end, we construct the manuscript as follows: In Sec. 2, we present a brief of the noncommutative effects on the black hole mass and lapse functions. Then, in Sec. 3, we examine the black hole thermodynamics. Next, in Sec. 4, we obtain the expected shadow images of the black hole. Then, in Sec. 5, discuss the QNMs. Finally, we conclude the manuscript.

2 A brief review

In this section, we aim to introduce the geometry of the noncommutative Schwarzschild black hole that is surrounded by the quintessence matter field. Here, noncommutativity can be taken as a correction to the Schwarzschild black hole metric and its contribution vanishes when its strength goes to zero, as defined in the simplest form below:

$$[X^\mu, X^\nu] = i\Theta^{\mu\nu}. \quad (5)$$

Here, $\Theta^{\mu\nu}$ is an antisymmetric constant tensor of dimension $(\text{length})^2$.

In commutative spacetime, one can represent a point particle’s mass density by an ordinary product of its mass with a Dirac delta function. However, in a noncommutative space, describing point mass in such a manner becomes impractical due to the inherent fuzziness of space resulting from the position-position uncertainty relation. In this case, the measure of this fuzziness has to be considered with the noncommutative parameter, Θ . In literature, various forms of mass density have been proposed

[143, 173–176]. In this manuscript, we employ the following distribution form [173]

$$\rho_{\text{matt}}(\Theta, r) = \frac{M\sqrt{\Theta}}{\pi^{3/2}(r^2 + \pi\Theta)^2}, \quad (6)$$

where M is the total mass defused throughout the region of linear size $\sqrt{\Theta}$. Now, in the presence of a quintessence matter field, we look for a static, spherically symmetric, asymptotically Schwarzschild black hole solution of the Einstein equations with the energy density defined above. We consider the spherically symmetric black hole metric of the form

$$\begin{aligned} ds^2 &= -e^\nu dt^2 + e^\mu dr^2 + r^2 d\Omega^2, \\ &= -f(r, \Theta, \omega_q) dt^2 + \frac{1}{f(r, \Theta, \omega_q)} dr^2 + r^2 d\Omega^2, \end{aligned} \quad (7)$$

with

$$f(r, \Theta, \omega_q) = 1 - \frac{2\mathcal{M}(r, \Theta, \omega_q)}{r}, \quad (8)$$

where μ and ν depend only on r with $\nu = -\mu$, and $\mathcal{M}(r, \Theta, \omega_q)$ represents the smear mass. We then express the Einstein equation with the following form

$$G_{\alpha\beta} = R_{\alpha\beta} - \frac{1}{2}g_{\alpha\beta}R = 2 \left(4\pi T_{\alpha\beta_{\text{matt}}}(r, \Theta) + T_{\alpha\beta_{\text{quin}}}(\omega_q) \right), \quad (9)$$

where we assume $G = c = \hbar = k_B = 1$. As shown by Kiselev in [34], we take the time component of the energy-momentum tensor for quintessence matter

$$T_{0_{\text{quin}}}^0(\omega_q) = \frac{3\omega_q\sigma}{2r^{3\omega_q+3}}, \quad (10)$$

and the stress-energy tensor component

$$T_{0_{\text{matt}}}^0(r, \Theta) = -\rho_{\text{matt}}(\Theta, r), \quad (11)$$

and employ them in Eq. (9). We find

$$G_0^0 = -8\pi\rho_{\text{matt}}(\Theta, r) + \frac{3\omega_q\sigma}{r^{3\omega_q+3}}. \quad (12)$$

To solve Eq. (12), we first need to determine the G_{00} component of the Einstein tensor. Using the metric, given in Eq. (7), we calculate it as:

$$G_{00} = e^\nu \left(\frac{1}{r^2} - e^{-\mu} \left(\frac{1}{r^2} - \frac{\mu'}{r} \right) \right) = f(r, \Theta, \omega_q) \left(\frac{2}{r^2} \frac{d\mathcal{M}(r, \Theta, \omega_q)}{dr} \right). \quad (13)$$

Thus, G_0^0 component reads:

$$G_0^0 = -\frac{2}{r^2} \frac{d\mathcal{M}(r, \Theta, \omega_q)}{dr}. \quad (14)$$

Then, we match Eqs. (12) and (14), and we get

$$\frac{d\mathcal{M}(r, \Theta, \omega_q)}{dr} = 4\pi r^2 \rho_{\text{matt}}(\Theta, r) - \frac{3\omega_q\sigma}{2r^{3\omega_q+1}}. \quad (15)$$

After we substitute the energy distribution, we integrate Eq. (15). We obtain the smeared mass distribution

$$\mathcal{M}(r, \Theta, \omega_q) = \frac{2M}{\pi} \left[\tan^{-1} \left(\frac{r}{\sqrt{\pi\Theta}} \right) - \frac{r\sqrt{\pi\Theta}}{r^2 + \pi\Theta} \right] + \frac{\sigma}{2r^{3\omega_q}}. \quad (16)$$

Therefore, the lapse function reads:

$$f(r, \Theta, \omega_q) = 1 - \frac{2M}{\pi} \left[\tan^{-1} \left(\frac{r}{\sqrt{\pi\Theta}} \right) - \frac{r\sqrt{\pi\Theta}}{r^2 + \pi\Theta} \right] - \frac{\sigma}{r^{1+3\omega_q}}, \quad (17)$$

and up to the first order of the noncommutative correction it becomes

$$f(r, \Theta, \omega_q) = 1 - \frac{2M}{r} + \frac{8M}{\sqrt{\pi}r^2} \sqrt{\Theta} - \frac{\sigma}{r^{3\omega_q+1}}. \quad (18)$$

It is worth noting that in the absence of the quintessence matter field, the last terms of Eqs. (16), (17) and (18) drop, so the smeared mass and the lapse functions become the same as given in [163, 173]. Moreover, for the commutative case, $\Theta \rightarrow 0$, Eq. (18) simplifies to the conventional Schwarzschild metric surrounded by quintessence [54].

Here, we should also note that for supermassive black holes, like six million solar mass one, spacetime can be treated as a smooth classical manifold since the effect of noncommutativity is negligible (commutative limit). However, for mini black holes [177], where quantum effects dramatically alter spacetime structure, substantial differences arise from spacetime fuzziness related to uncertainty principle considerations. One expects significant changes due to the spacetime fuzziness. Moreover, for $\frac{8M\sqrt{\Theta}}{\sqrt{\pi}} = Q^2$, the metric is largely similar to the Reissner-Nordström black hole surrounded with quintessence [178–180].

In Figure 1, we plot the lapse function versus r . To be more precise, in Figures (1a) and (1b) we demonstrate the impact of the quintessence field and noncommutativity by comparing the lapse function with the ordinary case one. Then, in Figures (1c) and (1d), we investigate whether a naked singularity exists or not for the two cases that we will use during the rest of the manuscript.

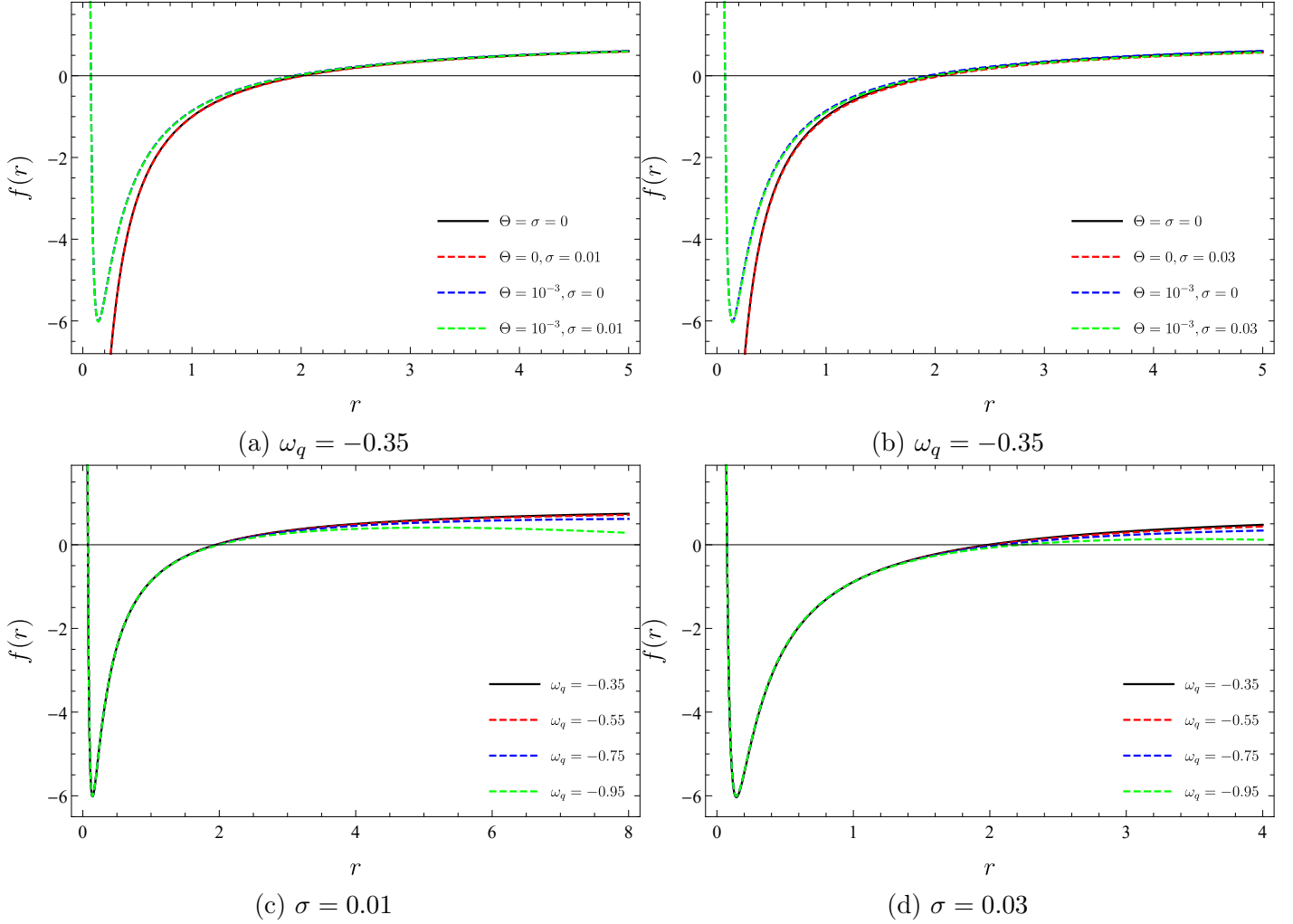


Figure 1: Variation of the lapse function with respect to r for $M = 1$.

Here, we have the following observations:

- For $\Theta = \sigma = 0$, the metric function matches with the standard Schwarzschild solution [145]. The well-known solution has a coordinate singularity at $r = 2M$ and it is free from naked singularity.
- Without noncommutativity, the quintessence matter-modified metric function mimics the ordinary case with a slight shift at greater radii values at relatively small radii. For example, for $\sigma = 0.01$ and $\sigma = 0.03$ with $\omega_q = -0.35$ the coordinate singularity appears at $r \simeq 2.02M$ and $r \simeq 2.06M$, respectively. In both cases, the event horizons cover the central singularity. Therefore, we conclude that these cases are also free of naked singularity.
- In the noncommutative case without the quintessence matter the lapse function approaches infinity as r tends to zero. This indicates the presence of a curvature singularity at the origin, $r = 0$, however, it is not detectable because of the fuzziness of the spacetime. In addition, we observe that the lapse function changes its sign at $r \simeq 1.93M$. This implies the existence of an event horizon at that radius which shows us that the central singularity is covered by the event horizon.
- In the noncommutative case with the quintessence matter the lapse functions mimic the previous case with a slight shift at relatively small radii and it approaches infinity as r tends to zero. For $\sigma = 0.01$ and $\sigma = 0.03$ with $\omega_q = -0.35$ the lapse functions change their sign at $r \simeq 1.95M$ and

$r \simeq 1.99M$, respectively. Like the previous case, we conclude that in this scenario the central singularity is appropriately covered by the event horizon.

- Figure (1c) for $\sigma = 0.01$ and Figure (1d) for $\sigma = 0.03$ confirm the existence of horizon radii for various quintessence state parameters. Since the model with these parameters does not contain any physically unacceptable naked singularities, we will use these parameters in the remainder of this article.

Then, for a specific quintessential state parameter, we determine the event horizon, r_H , via $f(r_H, \Theta) = 0$, and we express black hole mass function in terms of the event horizon in the presence of quintessence as

$$M_H(\omega_q, \Theta) = \frac{r_H}{2} \left(1 + \frac{4\sqrt{\Theta}}{\sqrt{\pi}r_H} + \frac{16\Theta}{\pi r_H^2} \right) \left(1 - \frac{\sigma}{r_H^{1+3\omega_q}} \right). \quad (19)$$

In Figure 2, we depict the mass function for a set of two different valued noncommutative and normalization constant parameters. In each plot, we consider four different quintessence state parameters which correspond to four distinct scenarios.

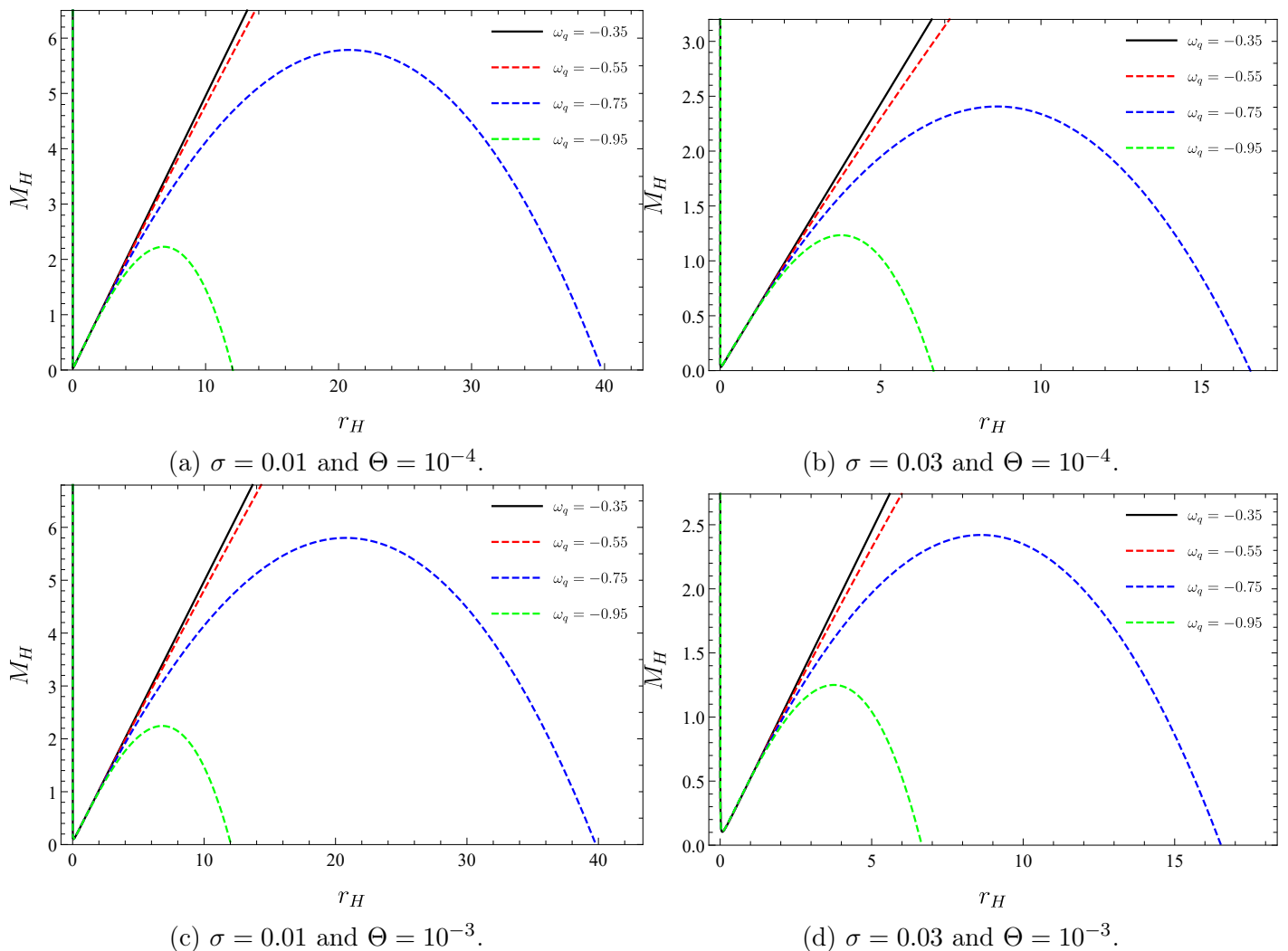


Figure 2: The effect of the quintessence matter on the black hole mass.

These qualitative plots show us that the quintessence matter alters the characteristics of the mass function as in the commutative case. As we know well, in the ordinary Schwarzschild black hole case,

the mass function has a linear relationship with the horizon radius, $M = \frac{r_H}{2}$. This relation sets forward that as the horizon radius leads to zero, the mass also approaches to zero, thus, the mass vanishes at the origin. However, in noncommutative spacetime due to fuzziness, there is a lower bound on the radius, which ensures that the black hole mass has a non-zero minimum mass value at a minimum event horizon radius. We observe that at relatively small horizon radii quintessence matter does not have an impact on the mass function. In the limit of $r_H \gg \sqrt{\Theta}$, the impact of noncommutative geometry disappears, however, the effects of the quintessence matter become dominant and it enforces a decrease in the rate of the mass increase [181]. This alteration ends at a maximum mass value, and then, the mass starts to decrease and it equals to zero at $r_H = \sigma^{\frac{1}{3\omega_q+1}}$.

3 Black Hole Thermodynamics

In this section, our focus will be on deriving the exact forms of various thermal quantities such as Hawking temperature, entropy, heat capacity, and Gibbs free energy. Our exploration begins with the Hawking temperature, which is usually defined by the following expression [4]

$$T = \frac{\kappa}{2\pi}, \quad (20)$$

where κ corresponds to the surface gravity and it can be deduced via

$$\kappa = - \sqrt{-\frac{g^{11}}{g^{00}} \frac{(g_{00})'}{g_{00}}} \Big|_{r=r_H}. \quad (21)$$

After performing the straightforward computations, we obtain the Hawking temperature with the non-commutative correction term in the form of

$$T_H(\omega_q, \Theta) = \frac{1}{4\pi r_H} \left(1 + \frac{3\sigma\omega_q}{r_H^{3\omega_q+1}} \right) - \frac{1}{\pi r_H^2} \left(\sqrt{\frac{\Theta}{\pi}} + \frac{4\Theta}{\pi r_H} \right) \left(1 - \frac{\sigma}{r_H^{3\omega_q+1}} \right). \quad (22)$$

When $\Theta = 0$, Eq. (22) simplifies to the same form found in [54].

$$T_H(\omega_q) = \frac{1}{4\pi r_H} \left(1 + \frac{3\sigma\omega_q}{r_H^{3\omega_q+1}} \right), \quad (23)$$

Furthermore, in the absence of the quintessence matter the noncommutative corrected Hawking temperature reduces to

$$T_H(\Theta) = \frac{1}{4\pi r_H} - \frac{1}{\pi r_H^2} \left(\sqrt{\frac{\Theta}{\pi}} + \frac{4\Theta}{\pi r_H} \right). \quad (24)$$

Finally, for the set of $\Theta = \sigma = 0$, the conventional result appears.

To get an appropriate description of the Hawking temperature behavior, in Figure 3 we illustrate the relationship between T_H and r_H for $\omega_q = -0.35$ and $\omega_q = -0.95$, respectively.

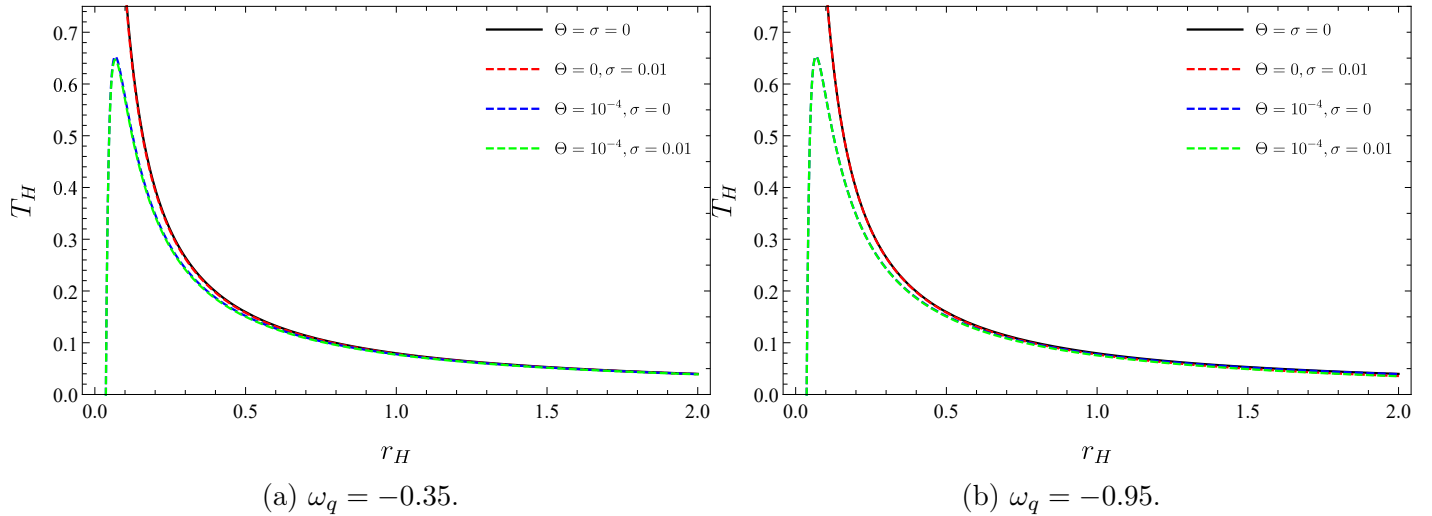


Figure 3: Hawking temperature versus event horizon radius of the noncommutative black hole surrounded by quintessence matter.

In ordinary case, as $r_H \rightarrow 0$, the Hawking temperature becomes infinite. This divergence of the Hawking temperature is known as the *divergence problem* or *infinite temperature problem*. This divergence implies that the black hole would emit an infinite amount of radiation as the black hole approaches to the Planck length, and the semiclassical approximation used to derive the Hawking radiation breaks down. It suggests that a full theory of quantum gravity, which should describe such extreme regimes, is needed to understand the behavior of black holes at these scales. Here, we see that the noncommutativity eliminates this divergence problem of the Hawking temperature. We note that the black hole temperature rises during its evaporation, and it reaches a peak value T_H^{\max} at a critical horizon radius value, and subsequently it decreases to zero rapidly.

Then, in Figure 4, we show the impact of the quintessence state parameter.

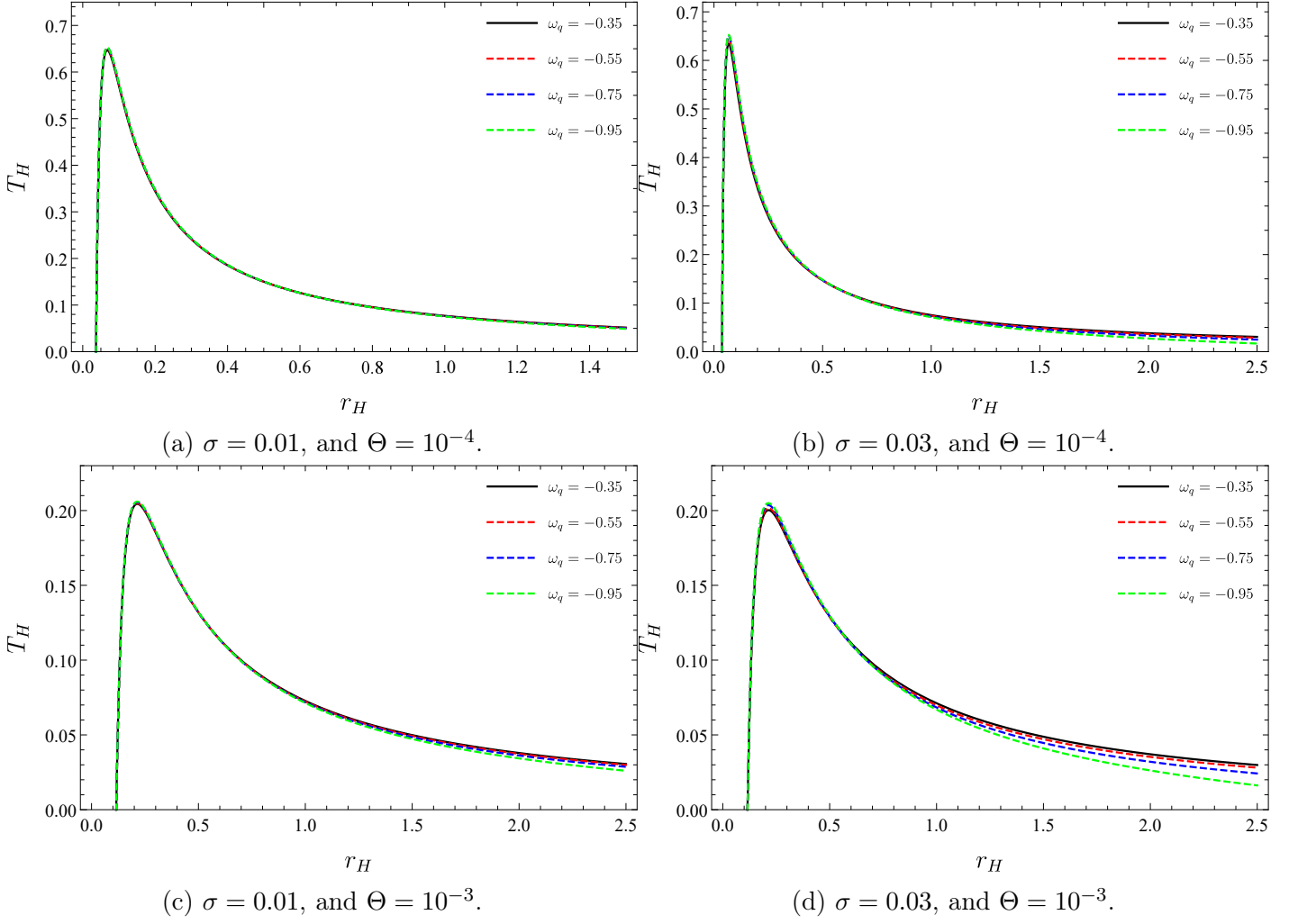


Figure 4: The qualitative effects of the noncommutative parameter and quintessence field on the black hole temperature.

We observe that the temperature has a maximum for all the values of Θ and σ such that for fixed ω_q when we increase the value of Θ or σ the local peak decreases. Next, we utilize the first law of black hole thermodynamics to derive the Bekenstein entropy, given by, $dS = \frac{dM}{T}$ [2, 3]. By using Eqs. (19) and (22), we get

$$S(\Theta) \simeq \frac{A}{4} + 4\sqrt{\Theta A} + 16\Theta \log \frac{A}{\ell_p^2}, \quad (25)$$

where $A_H = 4\pi r_H^2$ is the area of the event horizon, and ℓ_p is Planck length.

We notice that the noncommutative geometry always modifies the black hole entropy with a positively valued term. Unlike this effect, the presence of the quintessence matter does not alter the entropy. In Figure 5, we plot the noncommutative corrected entropy.

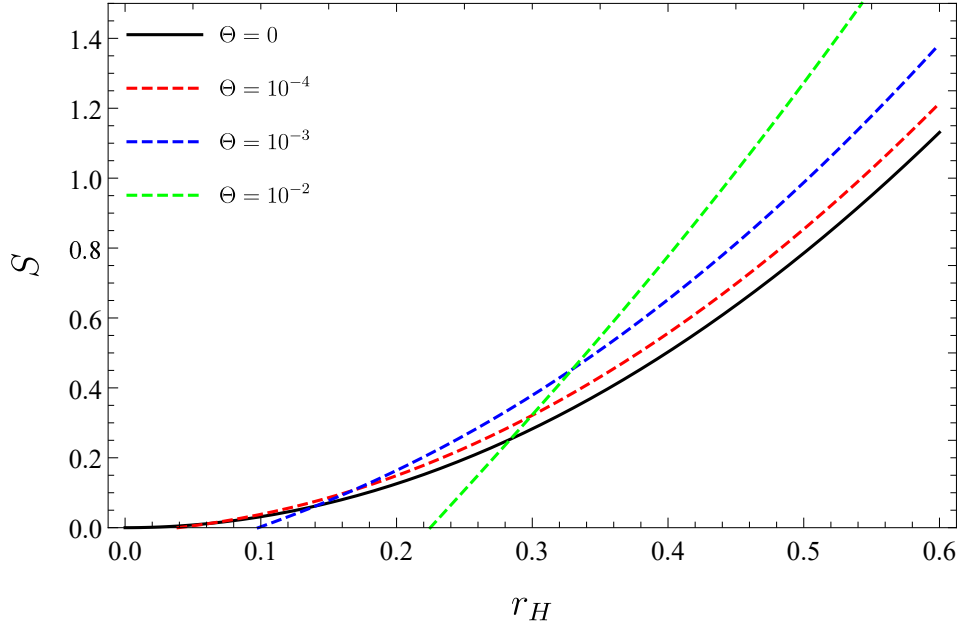


Figure 5: The effect of the noncommutative parameter on the entropy function.

We observe that the latter entropy function always takes greater values than its semi-classical form. Moreover, we see that depending to the noncommutativity parameter, the entropy become physically meaningful at different horizon. Next, we employ the following formula to derive the heat capacity function

$$C = \frac{dM_H}{dT_H}. \quad (26)$$

Using Eqs. (19) and (22), we obtain the noncommutative modified heat capacity in the form of

$$C(\omega_q, \Theta) = -\frac{2\pi r_H^2 \left(1 + \frac{3\sigma\omega_q}{r_H^{3\omega_q+1}}\right)}{1 + \frac{3\sigma\omega_q(3\omega_q+2)}{r_H^{3\omega_q+1}}} - \frac{16\sqrt{\pi\Theta}r_H \left(1 + \frac{\sigma(3\omega_q-1)}{r_H^{3\omega_q+1}} + \frac{3\sigma^2\omega_q(9\omega_q^2+6\omega_q-1)}{2r_H^{6\omega_q+2}}\right)}{\left(1 + \frac{3\sigma\omega_q(3\omega_q+2)}{r_H^{3\omega_q+1}}\right)^2} - \frac{192\Theta \left(1 + \frac{\sigma(3\omega_q^2+7\omega_q-4)}{2r_H^{3\omega_q+1}} - \frac{\sigma^2(27\omega_q^4-18\omega_q^3-15\omega_q^2+10\omega_q-2)}{2r_H^{6\omega_q+2}} + \frac{3\sigma^3\omega_q(27\omega_q^4+36\omega_q^3+3\omega_q^2-5\omega_q+1)}{2r_H^{9\omega_q+3}}\right)}{\left(1 + \frac{3\sigma\omega_q(3\omega_q+2)}{r_H^{3\omega_q+1}}\right)^3}. \quad (27)$$

For $\Theta = \sigma = 0$ the heat capacity function reduces to the well-know result, $C = -2\pi r_H^2$ [182]. We see that the heat capacity of the black hole is corrected by both parameters in a very complex structure. Therefore, we have to use numerical methods to analyze the effects of additive terms. To this end, we plot Figure 6 and illustrate the heat capacity's behavior for two different values of the quintessence state parameter. These figures show us the quintessence state parameter value has a critical role in black hole stability. For example, for the case $\omega_q = -0.35$ the BH is unstable, however, for $\omega_q = -0.95$ the heat capacity can be equal to zero at $r_H = r_{rem}$ so that black hole terminates the radiation and a remnant mass occurs. Moreover, for $r_H < r_{rem}$ the black hole has a negative heat capacity which signifies an unstable phase of the black hole. Similarly, for $r_H > r_{rem}$, the black hole becomes stable since it has a positive heat capacity.

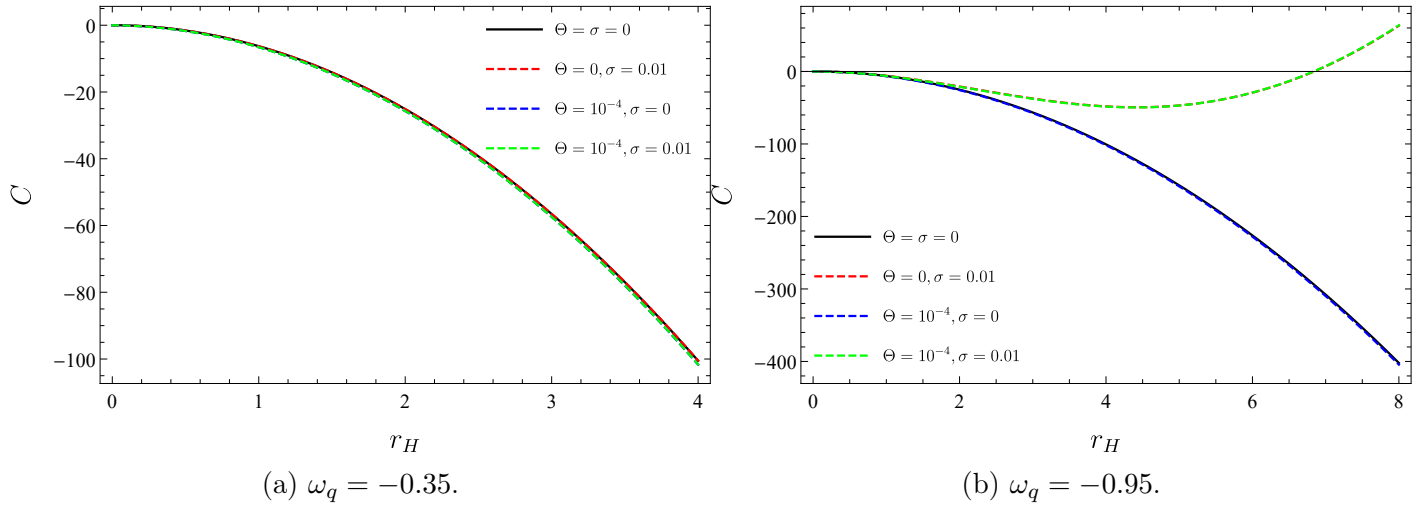


Figure 6: Heat capacity function versus event horizon radius of the noncommutative black hole surrounded by quintessence matter.

Figure 7 presents the impact of the quintessence field and noncommutative parameters on the black heat capacity. Similar to the mass and Hawking temperature cases, we use a set of two different valued noncommutative and normalization constant parameters. Moreover, in each plot, we employ the same four different quintessence state parameters which correspond to four distinct scenarios.

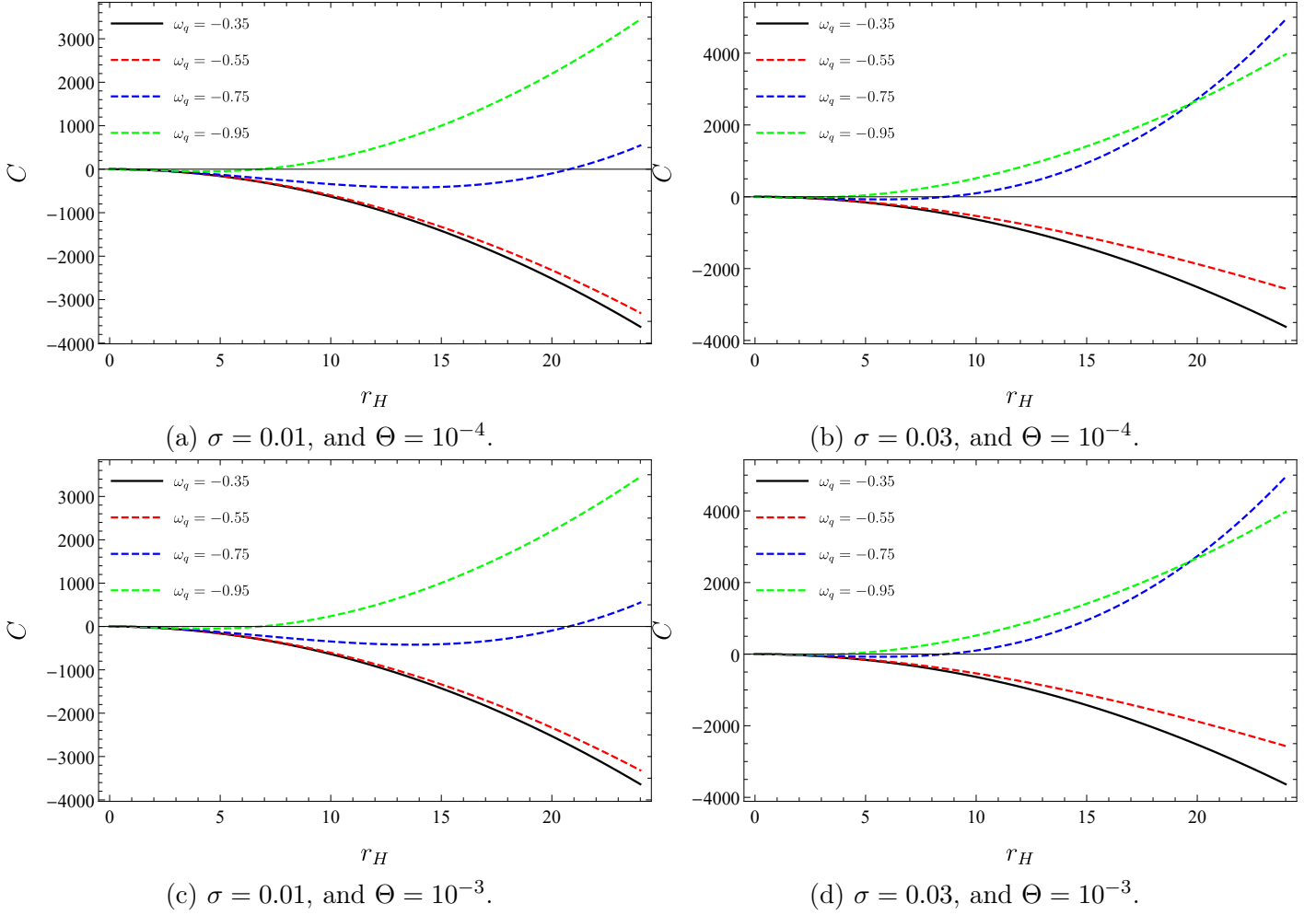


Figure 7: The influence of the noncommutative and quintessence state parameters on the heat capacity.

We observe that the effect of the noncommutative parameter and quintessence field are very significant. For additional details on the phase transition and overall stability, our focus turns to the Gibbs free energy, which is defined by

$$G = M - TS, \quad (28)$$

Substituting Eqs. (19), (22), and (25) into Eq. (28), we obtain

$$G(\omega_q, \Theta) = \frac{r_H}{4} \left(1 - \frac{\sigma(3\omega_q + 2)}{r_H^{1+3\omega_q}} \right) + \sqrt{\frac{\Theta}{\pi}} \left(1 - \frac{3\sigma(2\omega_q + 1)}{r_H^{1+3\omega_q}} \right) - \frac{4\Theta}{\pi} \left(\frac{2}{r_H} \left(1 + \frac{3\sigma\omega_q}{r_H^{3\omega_q+1}} \right) \log \frac{r_H}{\ell_p} - \frac{5}{r_H} \left(1 - \frac{\sigma}{r_H^{3\omega_q+1}} \right) \right). \quad (29)$$

In Figure 8, we depict the Gibbs free energy function versus event horizon.

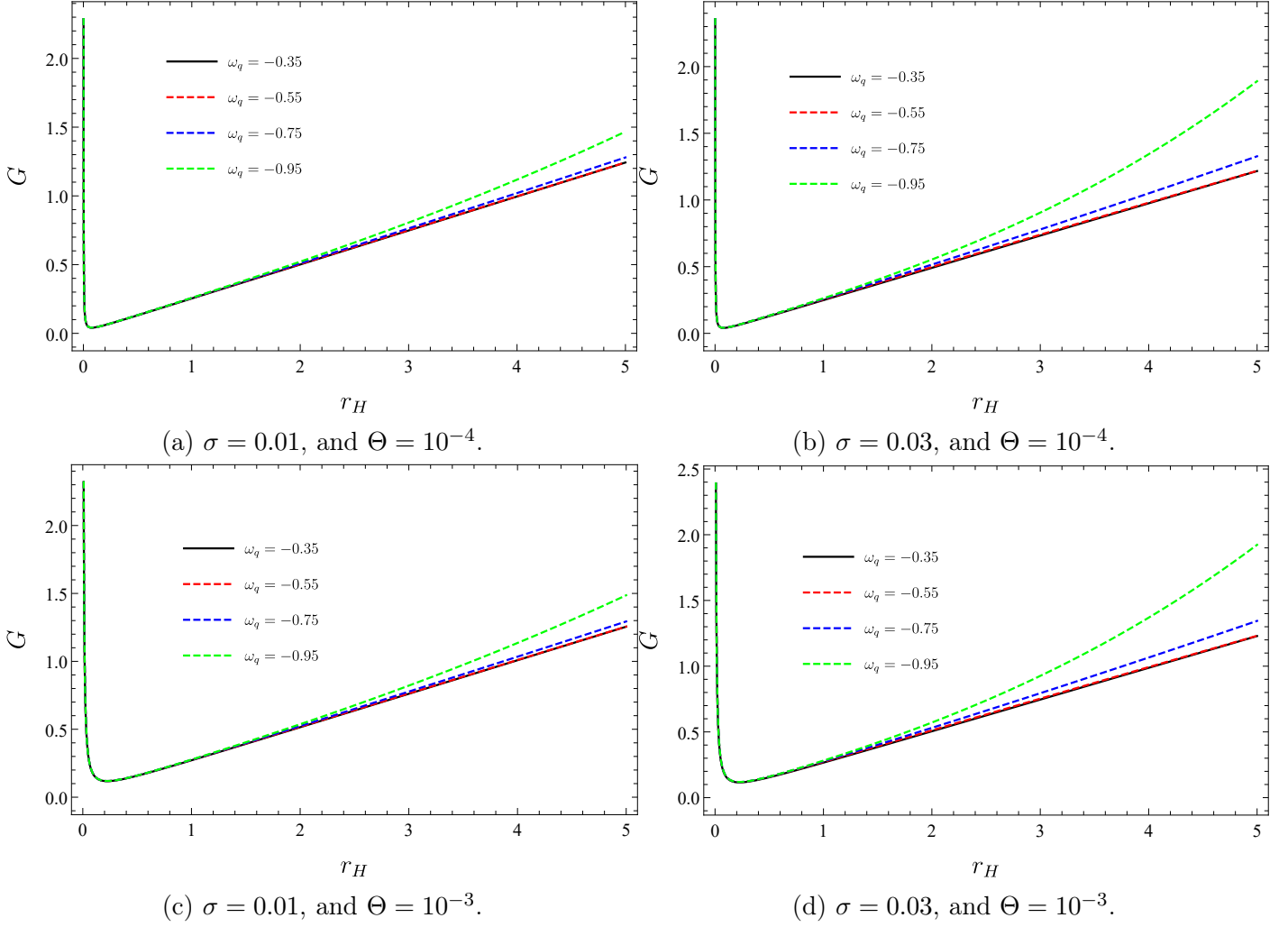


Figure 8: Gibbs free energy function versus event horizon radius of the noncommutative black hole surrounded by quintessence matter.

These figures show that the Gibbs free energy function has a turning point which can be determined via $\frac{\partial G}{\partial r_H} = 0$. Here, we observe that the location of that minimum value depends on the normalization factor associated with the quintessence field and noncommutative parameters.

4 Shadow in the presence of plasma

In this section, we assume a plasma distribution that surrounds the black hole with a refractive index, $n = n(x, \omega)$. Here, ω corresponds to the photon frequency measured by an observer that moves with a velocity u^α . In this case, the effective energy of the photon reads:

$$\hbar\omega = -p_\mu u^\mu. \quad (30)$$

In [183], the refractive index of the medium is given as a function of the photon four-momentum

$$n^2 = 1 + \frac{p_\mu p^\mu}{(p_\mu u^\mu)^2}. \quad (31)$$

In the vacuum scenario, $n = 1$, the standard condition for null geodesics is restored by $p_\mu p^\mu = 0$. Now, we consider a photon around a given spacetime geometry surrounding plasma. We express the

Hamiltonian, as given in [183]

$$H = \frac{1}{2} \left[g^{\mu\nu} p_\mu p_\nu - (n^2 - 1) \left(p_0 \sqrt{-g^{00}} \right)^2 \right]. \quad (32)$$

In [183, 184], authors noted that one can introduce a particular expression for the plasma frequency to facilitate analytical computations, under the assumption that the refractive index follows a general form,

$$n^2 = 1 - \frac{\omega_e^2}{\omega^2} = 1 - \frac{k}{r}, \quad k > 0. \quad (33)$$

Now, we have to introduce how to obtain the trajectories of photons. In terms of the affine parameter, τ , they are governed by the following set of equations:

$$\frac{\partial x^\mu}{\partial \tau} = \dot{x}^\mu = \frac{\partial}{\partial p_\mu} H, \quad (34)$$

$$\frac{\partial p_\mu}{\partial \tau} = \dot{p}_\mu = -\frac{\partial}{\partial x^\mu} H. \quad (35)$$

After simple manipulation, we write the components of the canonically conjugate momentum as follows:

$$E = p_0 = -\frac{f(r)}{n^2} \dot{t}, \quad (36)$$

$$L = p_\phi = r^2 \sin^2 \theta \dot{\phi}. \quad (37)$$

Here, E and L represent the energy and angular momentum of the photons, respectively. Then, we deduce the remaining two geodesic equations from the Hamilton-Jacobi equation,

$$\frac{\partial}{\partial \tau} S = -\frac{1}{2} \left[g^{\mu\nu} \frac{\partial S}{\partial x^\mu} \frac{\partial S}{\partial x^\nu} - (n^2 - 1) \left(\frac{\partial S}{\partial t} \sqrt{-g^{00}} \right)^2 \right]. \quad (38)$$

Using Eq. (18) in Eq. (38), we obtain

$$\frac{\partial}{\partial \tau} S = -\frac{1}{2} \left[-\frac{n^2}{f(r)} \left(\frac{\partial S}{\partial t} \right)^2 + f(r) \left(\frac{\partial S}{\partial r} \right)^2 + \frac{1}{r^2} \left(\frac{\partial S}{\partial \theta} \right)^2 + \frac{1}{r^2 \sin^2 \theta} \left(\frac{\partial S}{\partial \phi} \right)^2 \right]. \quad (39)$$

We then assume a separable Jacobi action solution

$$S = -Et + L\phi + S_\theta + S_r, \quad (40)$$

where S_r component depends only on r , while S_θ component relies only on θ . Then, by replacing Eq. (40) with Eq. (39), we arrive at

$$\frac{n^2}{f(r)} E^2 - f(r) \left(\frac{\partial S_r}{\partial r} \right)^2 - \frac{1}{r^2} \left[\left(\frac{\partial S_\theta}{\partial \theta} \right)^2 - \mathcal{K} + L^2 \cot^2 \theta \right] - \frac{1}{r^2} \left[\frac{L^2}{\sin^2 \theta} + \mathcal{K} - L^2 \cot^2 \theta \right] = 0, \quad (41)$$

where \mathcal{K} is the Carter constant. Then, we recast Eq. (41) as the following two separated equations

$$\left(\frac{\partial S_\theta}{\partial \theta} \right)^2 = \mathcal{K} - L^2 \cot^2 \theta, \quad (42)$$

$$f^2(r) \left(\frac{\partial S_r}{\partial r} \right)^2 = n^2 E^2 - \frac{f(r)}{r^2} (L^2 + \mathcal{K}). \quad (43)$$

Now, using the relation $\left(\frac{\partial S_\theta}{\partial \theta}\right) = p_\theta$, we obtain

$$\frac{\partial S_\theta}{\partial \theta} = r^2 \dot{\theta}. \quad (44)$$

Similarly, employing the relation $\left(\frac{\partial S_r}{\partial r}\right) = p_r$, we find

$$\frac{\partial S_r}{\partial r} = \frac{\dot{r}}{f(r)}. \quad (45)$$

Then, we substitute Eqs. (44) and (45) to Eqs. (42) and (43) to express the complete null geodesic equations

$$r^2 \dot{r} = \pm \sqrt{n^2 E^2 r^4 - r^2 f(r) (L^2 + \mathcal{K})} = \pm \sqrt{\mathcal{R}}, \quad (46)$$

$$r^2 \dot{\theta} = \sqrt{\mathcal{K} - L^2 \cot^2 \theta}. \quad (47)$$

Since the equations of motion rely on conserved quantities E , L and \mathcal{K} , it is advantageous to express them in terms of normalized parameters

$$\zeta = \frac{L^2}{E^2}, \quad \eta = \frac{\mathcal{K}}{E^2}. \quad (48)$$

By doing so, the radial equation, namely Eq., (46) can be reformulated into a more common form of

$$\left(\frac{\partial r}{\partial \tau}\right)^2 + V_{eff}(r) = 0, \quad (49)$$

with the effective radial potential

$$V_{eff}(r) = E^2 \left[\frac{f(r)}{r^2} (\zeta^2 + \eta) - n^2 \right]. \quad (50)$$

In Figures (9) and (10), we depict the impact of the photon's radial motion on the effective potential.

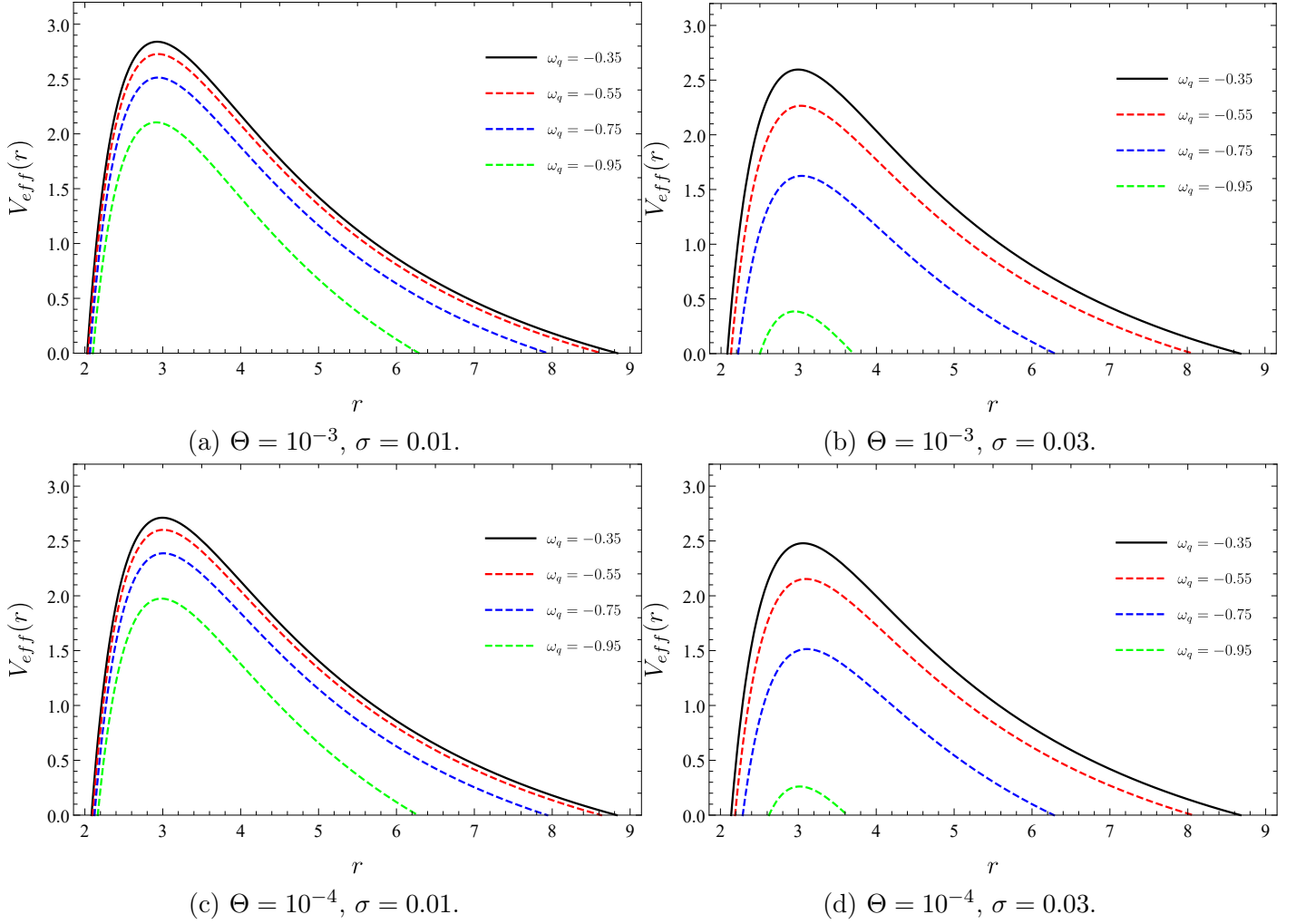


Figure 9: The variation of the effective potential as a function of the radial coordinate for two values of Θ and σ with $L = 10, \mathcal{K} = 1, E = 1, k = 0.1$.

Now, we explore the circular photon orbits. By definitions, they exist with the following two conditions

$$V_{eff}(r)|_{r=r_p} = 0, \quad (51)$$

$$\left. \frac{\partial V_{eff}(r)}{\partial r} \right|_{r=r_p} = 0. \quad (52)$$

Here, we also have to take the maximizing condition of the effective potential into account

$$\left. \frac{\partial^2 V_{eff}(r)}{\partial r^2} \right|_{r=r_p} < 0. \quad (53)$$

With the help of the first condition, given by Eq. (51), we realize that the impact parameters, ζ and η , should satisfy the following criteria

$$\zeta^2 + \eta = \frac{r_p^2 \left(1 - \frac{k}{r_p}\right)}{1 - \frac{2}{r_p} - \frac{\sigma}{r_p^{3\omega_q+1}}} - \frac{8\sqrt{\Theta} \left(1 - \frac{k}{r_p}\right)}{\sqrt{\pi} \left(1 - \frac{2}{r_p} - \frac{\sigma}{r_p^{3\omega_q+1}}\right)^2} + \frac{64\Theta \left(1 - \frac{k}{r_p}\right)}{\pi r_p^2 \left(1 - \frac{2}{r_p} - \frac{\sigma}{r_p^{3\omega_q+1}}\right)^2}, \quad (54)$$

while from the second condition, we find out

$$\left(n(r) r f'(r) - 2n(r) f(r) - 2r n'(r) f(r) \right) \Big|_{r=r_p} = 0. \quad (55)$$

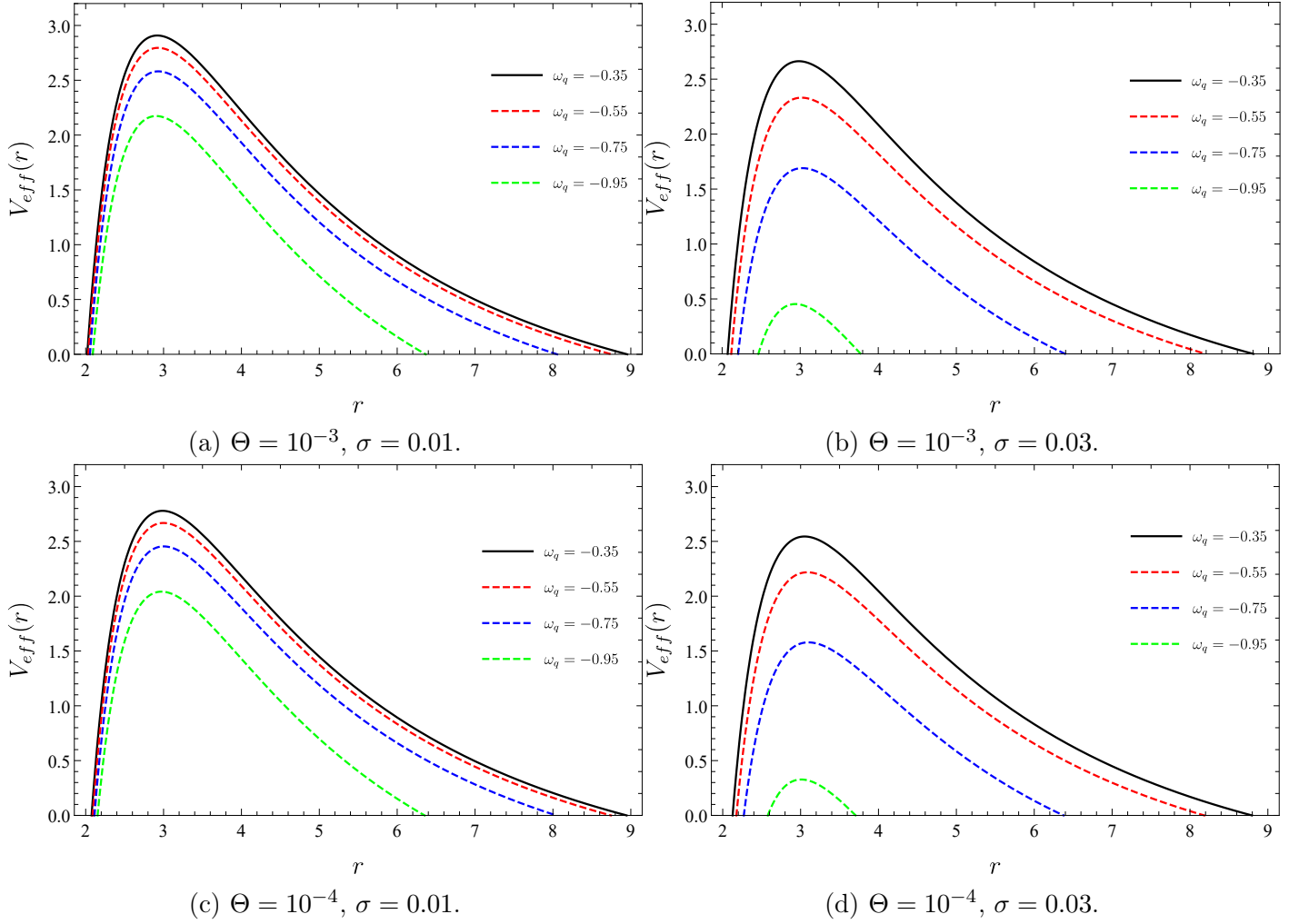


Figure 10: The variation of the effective potential as a function of the radial coordinate for two values of Θ and σ with $L = 10, \mathcal{K} = 1, E = 1, k = 0.3$.

Here, the prime sign denotes derivative with respect to r_p . Then, we utilize $f(r)$ and $n(r)$ expressions, given in Eqs. (18) and (33), to obtain an equation for the radius of the photon sphere. However, the resulting expression is intricate, and for brevity, we refrain from presenting it here. Therefore, we opt for a numerical solution. It is worth noting that the inclusion of the plasma medium introduces an additional parameter, k , in Eq. (55). For the numerical calculations, we consider different values for σ , ω_q , Θ , and k . Subsequently, we determine the values of the photon sphere radius and impact parameters numerically by solving Eq.(55). We tabulate our results in Tables 1 and 2.

We are now focusing on obtaining the black hole shadow with geodesic equations and criteria for unstable circular orbits. To facilitate this examination, we employ the celestial coordinates (X, Y) defined as [185]:

$$X = \lim_{r_o \rightarrow \infty} \left(-r_o^2 \sin \theta_o \frac{d\phi}{dr} \right), \quad (56)$$

$$Y = \lim_{r_o \rightarrow \infty} \left(r_o \frac{d\theta}{dr} \right), \quad (57)$$

where r_o corresponds to the distance between the observer and the black hole, while θ_o represents the angle of inclination between the observer's line of sight and the rotation axis of the black hole. Here,

	$\Theta = 10^{-3}, \sigma = 0.01$		$\Theta = 10^{-4}, \sigma = 0.01$		$\Theta = 10^{-3}, \sigma = 0.03$		$\Theta = 10^{-4}, \sigma = 0.03$	
ω_q	r_p	$\eta + \zeta^2$						
-0.35	2.91550	25.6359	2.98370	26.5396	2.98006	27.4024	3.04827	28.3481
-0.55	2.92592	26.4186	2.99471	27.3648	3.01541	30.2196	3.08550	31.3169
-0.75	2.92935	28.0477	2.99883	29.1102	3.02986	37.7032	3.10239	39.3848
-0.95	2.90408	31.7756	2.97306	33.1934	2.94601	72.5113	3.01670	79.5340

Table 1: Numerical estimations of the photon radius and the impact parameters for $k = 0.1$.

	$\Theta = 10^{-3}, \sigma = 0.01$		$\Theta = 10^{-4}, \sigma = 0.01$		$\Theta = 10^{-3}, \sigma = 0.03$		$\Theta = 10^{-4}, \sigma = 0.03$	
ω_q	r_p	$\eta + \zeta^2$						
-0.35	2.87819	23.8033	2.94693	24.6870	2.94287	25.4877	3.01160	26.4130
-0.55	2.88902	24.5373	2.95834	25.4621	2.97953	28.1344	3.05014	29.2064
-0.75	2.89410	26.0535	2.96413	27.0896	2.99960	35.1177	3.07271	36.7481
-0.95	2.87385	29.4984	2.94350	30.8707	2.93166	67.4244	3.00336	74.0682

Table 2: Numerical estimations of the photon radius and the impact parameters for $k = 0.3$.

the values of $\frac{d\phi}{dr}$ and $\frac{d\theta}{dr}$ can be determined by the geodesic equations given in Eqs. (37), (46) and (47):

$$\frac{d\phi}{dr} = \frac{\zeta}{r^2 \sin^2 \theta \sqrt{n^2 - \frac{f(r)}{r^2} (\zeta^2 + \eta)}}, \quad (58)$$

$$\frac{d\theta}{dr} = \frac{1}{r^2} \frac{\sqrt{\eta - \zeta^2 \cot^2 \theta}}{\sqrt{n^2 - \frac{f(r_o)}{r^2} (\zeta^2 + \eta)}}. \quad (59)$$

Substituting these equations into the definitions of X and Y , and taking the limit $r_o \rightarrow \infty$, we acquire:

$$X = -\zeta, \quad (60)$$

$$Y = \sqrt{\eta - \zeta^2 \cot^2 \theta_o}. \quad (61)$$

Next, for simplicity, we assume the observer on the equatorial plane, thus $\theta_o = \frac{\pi}{2}$. Then, these equations undergo simplification.

$$X = -\zeta, \quad Y = \sqrt{\eta}. \quad (62)$$

Using Eq. (54), one can read Eq. (62) as

$$X^2 + Y^2 = \zeta^2 + \eta = R_s^2. \quad (63)$$

Here, the quantity R_s is known as the radius of the shadow. Now, we aim to demonstrate the impact of the fuzziness and the quintessence matter parameters on the shadow of the black hole. First, we depict Figure 11.

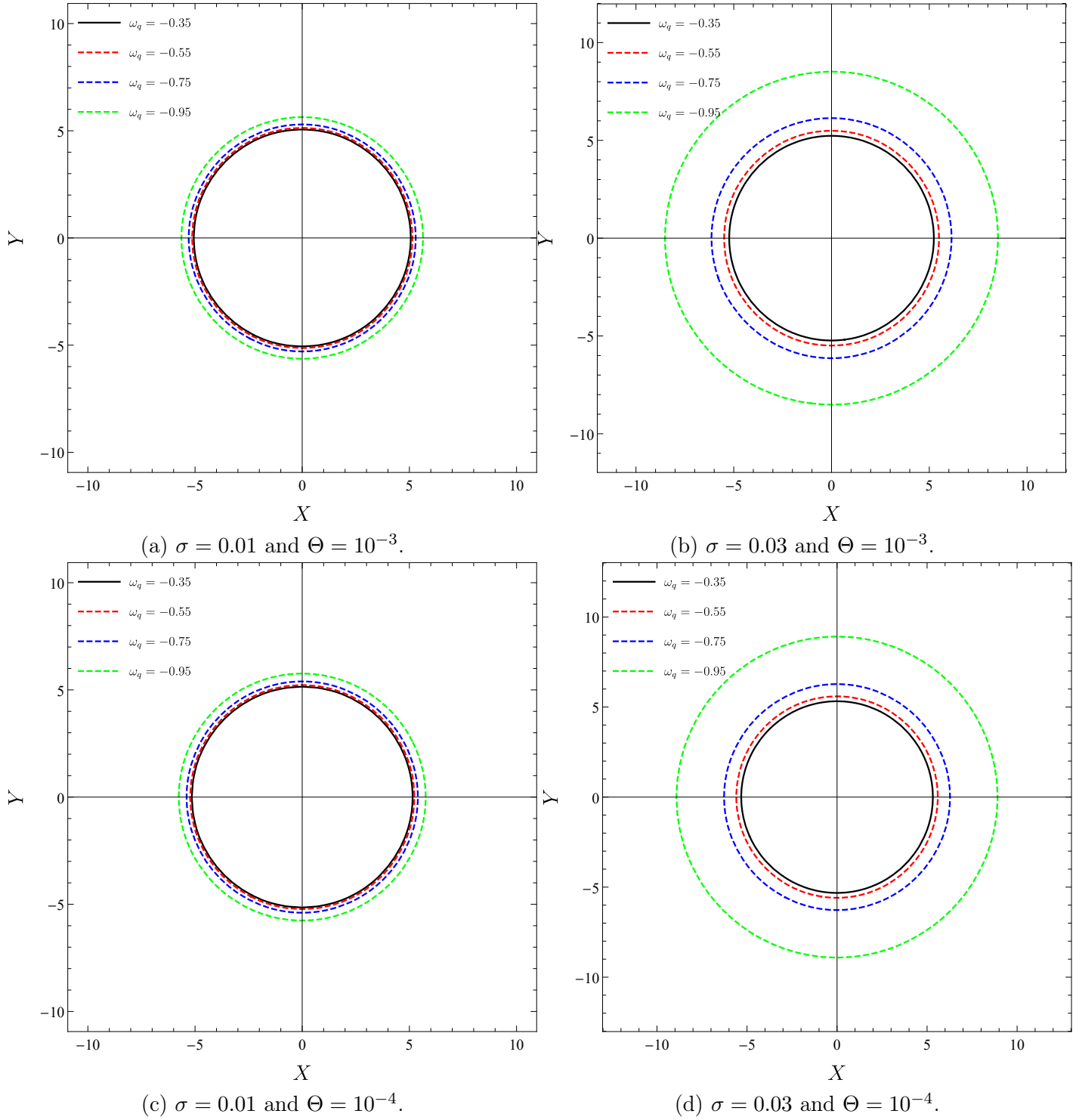


Figure 11: Black hole shadow in the celestial plane (X - Y) for different values of ω_q and $k = 0.1$.

Figure (11a) shows us that for a constant value Θ and σ we should observe a larger shadow radius at smaller quintessence state parameter values. Moreover, Figure (11b) tells us that for higher σ values the shadow radius grows significantly. However, Figure (11) cannot reveal the effect of noncommutative spacetime. To shed light on the noncommutativity effect, we show black hole shadows in Figure (12) for four different constant quintessence state parameters.

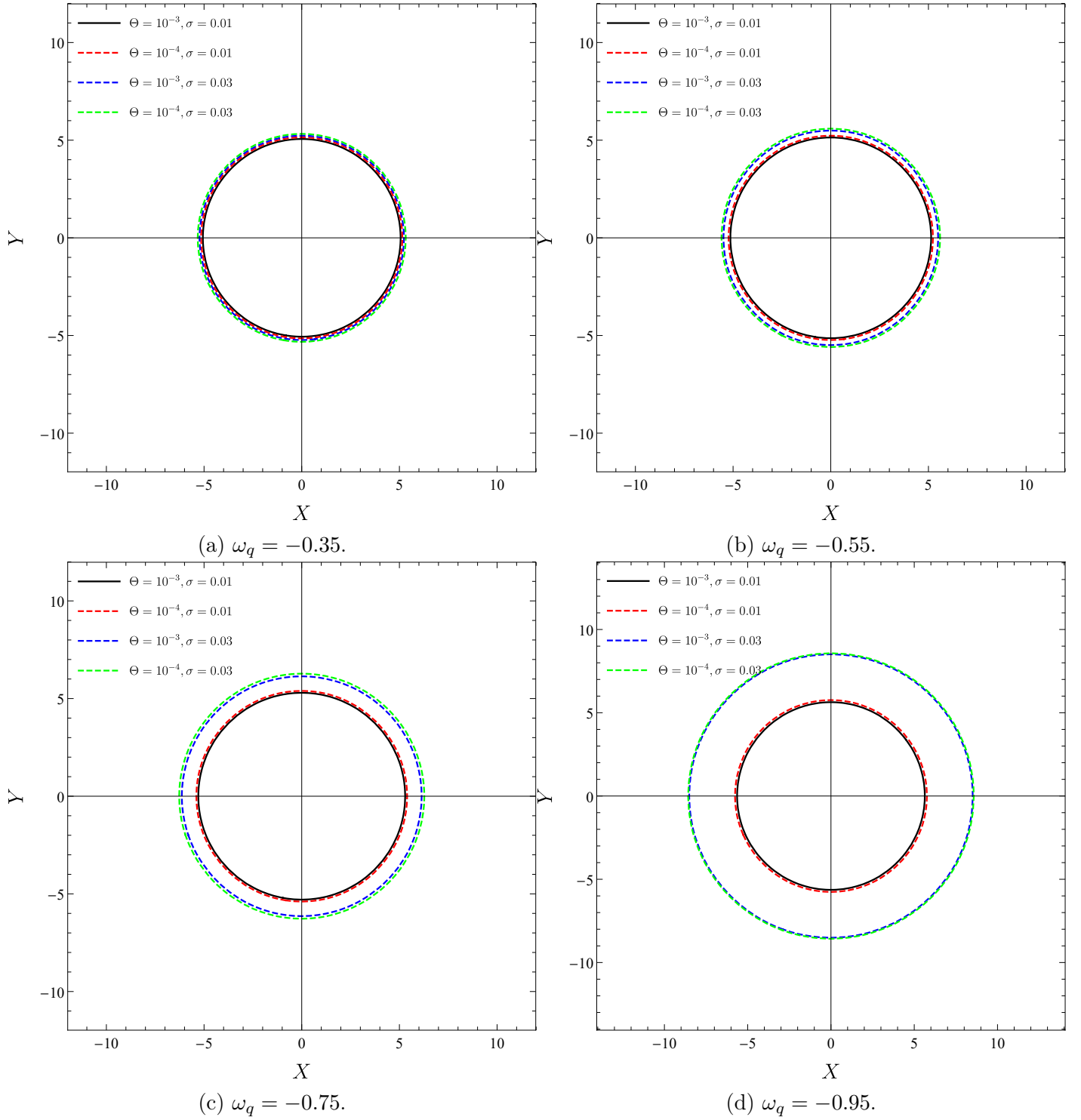


Figure 12: Black hole shadow in the celestial plane (X - Y) for different values of Θ and σ with $k = 0.1$.

We observe that for smaller noncommutativity parameters the shadow radius become slightly greater. We see that this effect remains the same at smaller quintessence state parameters.

5 Quasinormal modes

In general, the QNMs can be derived within two methodologies: perturbing the metric [186, 187], or coupling fields to the spacetime and considering the interactions between the black hole and the fields [188–192]. In this manuscript, we will follow the second methodology.

5.1 Wentzel - Kramers - Brillouin approximation

In this section, we explore the QNMs of the noncommutative Schwarzschild black hole surrounded by quintessence for a scalar field. We assume that the scalar field's influence on the black hole spacetime is insignificant, implying a negligible back reaction. Our approach to examining QNMs involves initially examining the Klein-Gordon equation and subsequently transforming it into a Schrödinger-like equation form. In the case of a massless scalar field, we first write the Klein-Gordon equation

$$\frac{1}{\sqrt{-g}}\partial_\mu(\sqrt{-g}g^{\mu\nu}\partial_\nu\psi) = 0, \quad (64)$$

we then employ the separating variables method with the following assumption:

$$\psi(t, r, \theta, \varphi) = e^{-i\omega t} \frac{\Psi_{\omega, L}(r)}{r} Y_{L, \mu}(\theta, \varphi), \quad (65)$$

where ω is the frequency, and $Y_{L, \mu}(\theta, \varphi)$ are the spherical harmonics. By inserting the described decomposition into Eq. (64), we get a Schrödinger like equation:

$$\frac{d^2}{dr^{*2}}\Psi(r^*) - (\omega^2 - \mathcal{V}(r))\Psi(r^*) = 0, \quad (66)$$

with the tortoise variable, $dr^* = \frac{dr}{f(r)}$, and

$$\mathcal{V}(r) = \frac{f(r)}{r} \frac{df(r)}{dr} + \frac{f(r)L(L-1)}{r}. \quad (67)$$

To solve Eq. (66), it is necessary to take suitable boundary conditions into account. In this scenario, acceptable solutions are those that are purely ingoing near the horizon:

$$\Psi \simeq e^{\pm i\omega r^*}, \quad r^* \rightarrow \pm\infty. \quad (68)$$

Now, we employ the WKB approximation to calculate the QNMs. Before giving the results, we would like to mention that the pioneering work using the WKB approximation to evaluate the QNMs was done by Schutz and Will [193]. Later, others extended the approximation to higher orders [194–196]. Following [195, 196], one can obtain the frequencies of QNMs with the following formula:

$$i \frac{(\omega - V_0)}{\sqrt{-2V_0''}} - \sum_{i=2}^N \Lambda_i = n + \frac{1}{2}. \quad (69)$$

Here, V_0 and V_0'' denote effective potential's height, and the second derivative with respect to the tortoise coordinate of the potential at its maximum " r_0^* ", respectively. Additionally, Λ_i is a constant coefficient resulting from higher order WKB corrections, and $n = 0, 1, 2, \dots$, is the overtone number. It is worth noting that the explicit expressions of Λ_i for higher orders are given in [195, 196].

We then utilize Eq. (69) to compute quasinormal frequency values with scalar field perturbations across different angular momentum and quintessence matter field parameter by using Padé averaged

L	n	$\omega_q = -0.35$	$\omega_q = -0.55$	$\omega_q = -0.75$	$\omega_q = -0.95$
1	0	0.268812 - 0.103954 i	0.264652 - 0.101739 i	0.256376 - 0.098084 i	0.248113 - 0.094897 i
2	0	0.466582 - 0.102567 i	0.459427 - 0.100353 i	0.445267 - 0.096690 i	0.416550 - 0.091167 i
	1	0.434087 - 0.379566 i	0.429369 - 0.370736 i	0.420170 - 0.356835 i	0.408909 - 0.337193 i
3	0	0.658273 - 0.099810 i	0.648278 - 0.097661 i	0.628470 - 0.094104 i	0.588260 - 0.088741 i
	1	0.669246 - 0.326342 i	0.658983 - 0.318950 i	0.639112 - 0.306561 i	0.600805 - 0.286269 i
	2	0.743689 - 0.489463 i	0.731238 - 0.479461 i	0.707431 - 0.462567 i	0.660694 - 0.436178 i
4	0	0.850307 - 0.098189 i	0.837430 - 0.096083 i	0.811909 - 0.092595 i	0.760102 - 0.087343 i
	1	0.858471 - 0.308954 i	0.845306 - 0.302195 i	0.819498 - 0.290890 i	0.768118 - 0.273022 i
	2	0.899347 - 0.570692 i	0.884810 - 0.556975 i	0.858113 - 0.534023 i	0.808330 - 0.444512 i
	3	0.977143 - 0.678626 i	0.960660 - 0.664834 i	0.929234 - 0.641516 i	0.867694 - 0.605089 i

Table 3: The QNMs of the noncommutative Schwarzschild black hole surrounded by quintessence for the massless scalar perturbation with $M = 1$, $\Theta = 10^{-4}$ and $\sigma = 0.01$ using the Pade averaged 6th order WKB approximation method.

6th order WKB approximation method. It is important to note that, according to the WKB formula, the best accuracy is achieved for $L > n$ [66]. Consequently, we exclusively examine scalar field functions that adhere to this condition, as they are associated with the low-lying QNMs. We tabulate our results in Table 3.

In Figure 13, we compare the variation of real and imaginary components of the quasinormal frequencies versus σ , considering two different cases.

We observe that with higher quintessence parameters both parts of the frequencies decrease. This means that the presence of the quintessence matter damps the oscillations. Then, we repeat the a similar comparison based on the angular momentum in Figure 14, and the quintessence state parameter in Figure 15, respectively. We conclude that the presence of the quintessence matter field alters the frequencies.

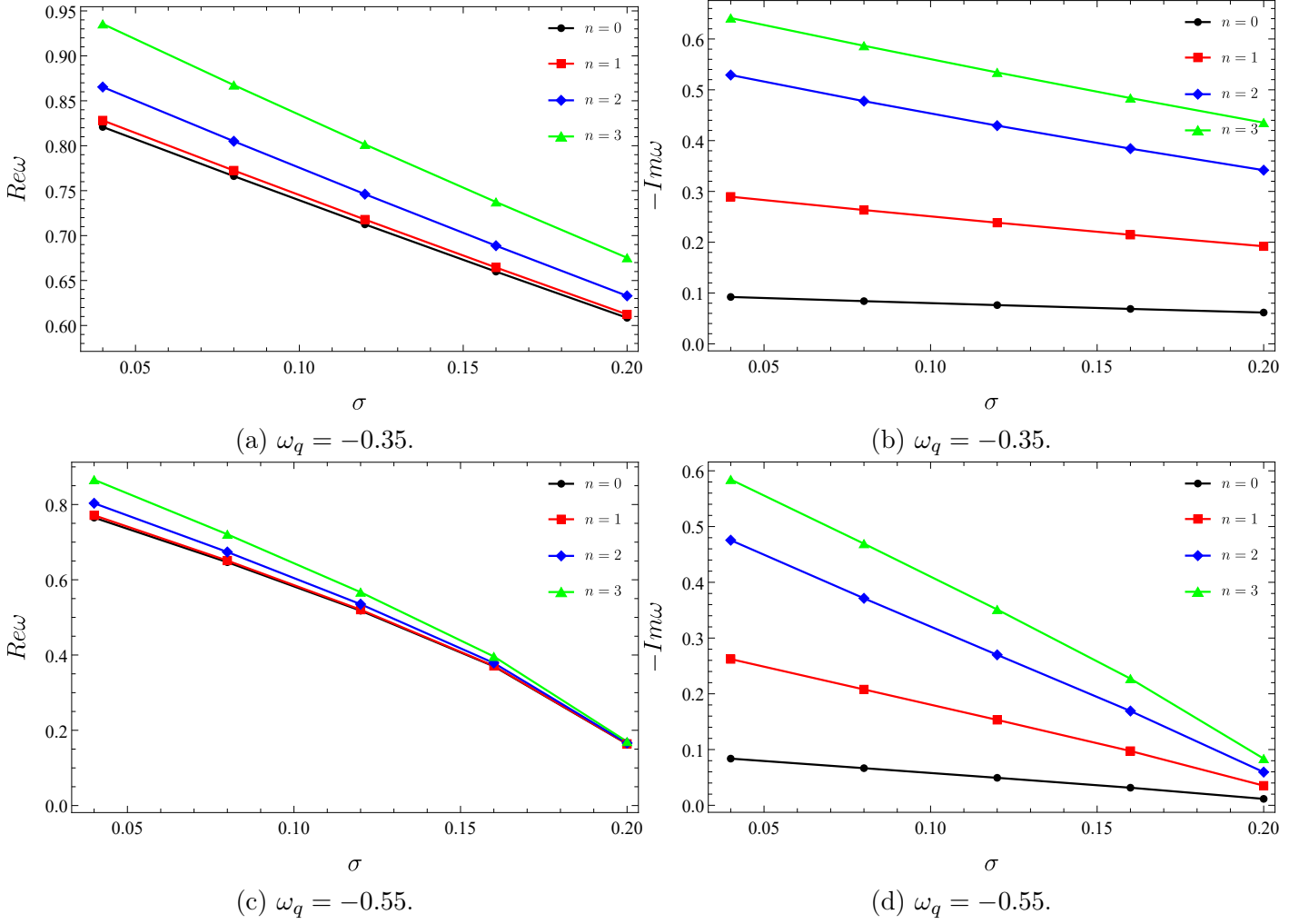


Figure 13: The variation of the $\text{Re } \omega$ and $\text{Im } \omega$ versus σ for two values of $\omega_q = -0.35, -0.55$ with $\Theta = 10^{-4}$.

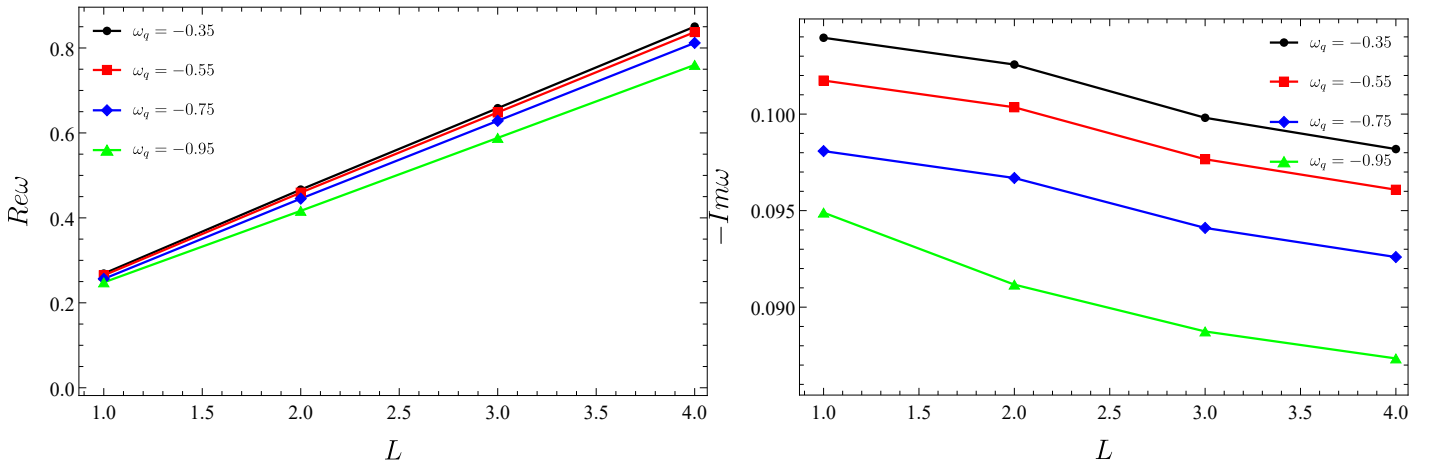


Figure 14: The variation of the $\text{Re } \omega$ and $\text{Im } \omega$ versus L for $\sigma = 0.01$, $n = 0$ and $\Theta = 10^{-4}$.

As we know, the WKB order plays a crucial role in obtaining the accurate values of QNMs frequencies. Increasing the order typically leads to improved approximations. However, this trend doesn't hold when we raise the multipole number. This observation becomes evident through the error estimation

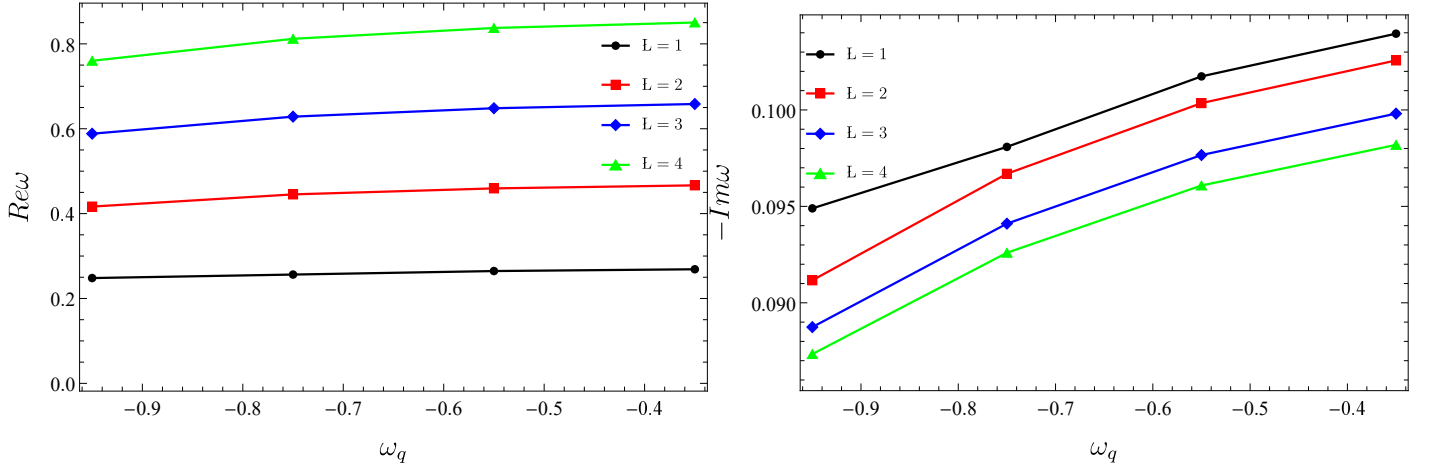


Figure 15: The variation of the $\text{Re } \omega$ and $\text{Im } \omega$ versus ω_q for $\sigma = 0.01$, $n = 0$ and $\Theta = 10^{-4}$.

associated with each order of the WKB formula. This error quantity for ω_k , derived from the WKB formula of order k for each overtone n , is defined as:

$$\Delta_k = \frac{|\omega_{k+1} - \omega_{k-1}|}{2}. \quad (70)$$

Using the definition, we present the calculated error estimation in Table 4.

	$\omega_q = -0.35$		$\omega_q = -0.55$	
k	ω_k	Δ_k	ω_k	Δ_k
3	0.820625 - 0.0911553 i	0.00639599	0.781027 - 0.085026 i	0.00584784
4	0.821186 - 0.0960695 i	0.00347966	0.781522 - 0.089458 i	0.00311287
5	0.826060 - 0.0955027 i	0.00433174	0.785848 - 0.088966 i	0.00379935
6	0.825272 - 0.0884303 i	0.00753273	0.785173 - 0.082794 i	0.00648148
7	0.812089 - 0.0898658 i	0.01604200	0.773872 - 0.084003 i	0.00648148
8	0.815841 - 0.1190980 i	0.03899340	0.776933 - 0.108640 i	0.03252780
9	0.887570 - 0.1094730 i	0.11296100	0.836701 - 0.100879 i	0.09267570
	$\omega_q = -0.75$		$\omega_q = -0.95$	
3	0.696617 - 0.0743361 i	0.00492351	0.490084 - 0.0538299 i	0.00326404
4	0.697008 - 0.0779159 i	0.00246121	0.490306 - 0.0558108 i	0.00125508
5	0.700350 - 0.0775440 i	0.00285470	0.491825 - 0.0556384 i	0.00157382
6	0.699858 - 0.0729691 i	0.00465141	0.491631 - 0.0538938 i	0.00116516
7	0.691827 - 0.0738162 i	0.00933632	0.489036 - 0.0541798 i	0.00267457
8	0.693824 - 0.0906397 i	0.02164900	0.489573 - 0.0588313 i	0.00536645
9	0.733450 - 0.0857426 i	0.05924060	0.499175 - 0.0576996 i	0.01252900

Table 4: QNMs of the massless scalar field for $M = 1$, $\sigma = 0.03$, $\Theta = 10^{-4}$ and $L = 4$, $n = 0$ calculated with the WKB formula of different orders.

5.2 Mashhoon approximation

The Mashhoon method [197], involves the approximation of the potential $\mathcal{V}(r^*)$ by using a potential with a comparable shape, for which the solutions of equation (66) can be evaluated analytically. This condition is met by employing the Pöschl-Teller (PT) potential, which has the form

$$\mathcal{V}(r^*) \sim V_{PT}(r^*) = \frac{V_0}{\cosh^2 \alpha (r^* - r_0^*)}. \quad (71)$$

Here, α is the curvature of the potential $\mathcal{V}(r^*)$ at its maximum $r^* = r_0^*$. Thus

$$\alpha = \sqrt{\left. \frac{-1}{2V_0} \frac{d^2 \mathcal{V}(r^*)}{dr^{*2}} \right|_{r^*=r_0^*}}. \quad (72)$$

Solving Eq. (66) with the PT approximation leads to the following equation for the calculation of QNMs [198]

$$\omega = \pm \alpha \sqrt{\frac{V_0}{\alpha^2} - \frac{1}{4}} + i\alpha \left(n + \frac{1}{2} \right). \quad (73)$$

We compute the QNMs using the Mashhoon approximation via Eq. (73). We tabulate the results in Table 5, and subsequently we compare them with ones obtained through the WKB method.

	$\omega_q = -0.35$		$\omega_q = -0.90$	
$\Theta \times 10^{-4}$	WKB method	Mashhoon appr.	WKB method	Mashhoon appr.
1	0.289890-0.117280 i	0.275811-0.0902164 i	0.0602218-0.0244681 i	0.0574887-0.0200356 i
2	0.290632-0.117272 i	0.276638-0.0902846 i	0.0634264-0.0257514 i	0.0605687-0.0210856 i
4	0.291696-0.117255 i	0.277826-0.0903789 i	0.0678057-0.0274948 i	0.0647827-0.0225133 i
6	0.292526-0.117237 i	0.278753-0.0904494 i	0.0710663-0.0287839 i	0.0679237-0.0235701 i
8	0.293233-0.117218 i	0.279545-0.0905075 i	0.0737591-0.0298420 i	0.0705202-0.0244384 i
10	0.293864-0.117198 i	0.280252-0.0905576 i	0.0760948-0.0307546 i	0.0727743-0.0251882 i

Table 5: Comparison of QNMs for a scalar field of noncommutative Schwarzschild black hole surrounded by quintessence, derived through the Mashhoon approximation and 3rd order WKB method, for specific parameters: $M = 1$, $L = 1$, $\sigma = 0.05$, and varying values of the parameter Θ .

6 Conclusion

In this work, we intended to investigate thermodynamics, shadows, and QNMs features of the Schwarzschild black hole surrounded by the quintessence matter in noncommutative spacetime. To achieve our goal, we first introduced the lapse function of the black hole, and then, we found the smeared mass function in terms of the event horizon. In four different scenarios of quintessence matter fields, we demonstrated the mass function's characteristics. We found that the event horizon has an upper bounded value depending on the quintessence matter field. Next, we obtained the Hawking temperature and verified our result with the ones that exist in the literature by considering the limit values of the scenarios. We noticed that the noncommutativity eliminates the divergence problem of the Hawking temperature. In addition, we noted that the black hole temperature rises during its evaporation, and it reaches a peak value T_H^{\max} at a critical horizon radius value, and subsequently, it decreases to zero rapidly. Then, we derived the entropy function and observed that the quintessence matter does not alter

its form, however, noncommutative effects do with a positive valued contribution. Next, we studied the heat capacity function. Its complex form allowed us to discuss its characteristics only numerically. We observed that the quintessence state parameter value has a critical role in black hole stability. In some scenarios, we found that the black hole can only be in the unstable state, but in other scenarios, we noted both the unstable and stable states of the black hole. We have also determined that the black hole radiation will terminate and a remnant mass will form. To understand whether the stability is local or global, we considered the Gibbs function and noted that the turning point varies depending on both the quintessence matter and noncommutative effects. Next, we studied the shadows by considering plasma distribution. After we obtained the effective potential, we showed the impact of the quintessence matter on the potential and shadows. Moreover, following the numerical calculations, we tabulated the photon radius and impact parameters. In the final section, we studied QNMs with WKB approximation. We observed the damping effects of the quintessence matter on real and imaginary parts of frequencies. After visualizing our results, we compared the QNMs modes with those obtained with the Mashhoon approach.

Acknowledgments

The authors are thankful to the anonymous reviewers for their constructive comments. B. C. L. is grateful to Excellence project PřF UHK 2211/2023-2024 for the financial support.

Data Availability Statements

The authors declare that the data supporting the findings of this study are available within the article.

References

- [1] J. D. Bekenstein, *Phys. Rev. D* **7**, 2333 (1973).
- [2] S. W. Hawking, *Commun. Math. Phys.* **25**, 152 (1972).
- [3] J. M. Bardeen, B. Carter, S. W. Hawking, *Commun. Math. Phys.* **31**, 161 (1973).
- [4] S. W. Hawking, *Commun. Math. Phys.* **43**, 199 (1975).
- [5] S. Carlip, *Int. J. Mod. Phys. D* **23**(11), 1430023 (2014).
- [6] D. N. Page, *New J. Phys.* **7**, 203 (2005).
- [7] A. Belhaj, M. Chabab, H. El Moumni, M. B. Sedra, *Chinese Phys. Lett.* **29** 100401 (2012).
- [8] M. Appels, R. Gregory, D. Kubizňák, *Phys. Rev. Lett.* **117**, 131303 (2016).
- [9] M. Appels, R. Gregory, D. Kubizňák, *J. High Energ. Phys.* **2017**, 116 (2017).
- [10] H. Hassanabadi, E. Maghsoodi, W. S. Chung, M. de Montigny, *Eur. Phys. J. C* **79**, 936 (2019).
- [11] R. André, J. P. S. Lemos, *Phys. Rev. D* **102**, 024006 (2020).
- [12] J. I. Musmarra, M. Bellini, M. Anabitarte, *Phys. Scr.* **96**, 065304 (2021).

- [13] B. Hamil, B. C. Lütfüoğlu, Eur. Phys. J. Plus **137**, 1124 (2022).
- [14] S. Wu, C. Liu, Nucl. Phys. B **985**, 115987 (2022).
- [15] B. Hamil, B. C. Lütfüoğlu, L. Dahbi, Int. J. Mod. Phys. A **37**, 2250130 (2022).
- [16] M. R. Khosravipoor, M. Farhodi, Eur. Phys. J. C **83**, 1045 (2023).
- [17] D. Wu, S. -Q. Wu, Phys. Rev. D **107**, 084002 (2023).
- [18] J. Sadeghi, M. A. S. Afshar, S. Noori Gashti, M. R. Alipour, Phys. Scr. **99**, 025003 (2024).
- [19] A. G. Riess et al., Astronom. J. **116**, 1008 (1998).
- [20] A. G. Riess et al., Astronom. J. **117**, 707 (1999).
- [21] S. J. Perlmutter et al., Astrophys. J. **517**, 565 (1999).
- [22] S. M. Carroll, Living Rev. Relativ. **4**, 1 (2001).
- [23] P. J. E. Peebles, B. Ratra, Rev. Mod. Phys. **75**, 559 (2003).
- [24] S. M. Carroll, Phys. Rev. Lett. **81**, 3067 (1998).
- [25] C. Armendariz-Picon, V. Mukhanov, P. J. Steinhardt, Phys. Rev. Lett. **85**, 4438 (2000).
- [26] T. Padmanabhan, Phys. Rev. D **66**, 021301 (2002).
- [27] R. R. Caldwell, Phys. Lett. B **545**, **23** (2002).
- [28] M. Gasperini, M. Piassa, G. Veneziano, Phys. Rev. D **65**, 023508 (2002).
- [29] J. Khoury, A. Weltman, Phys. Rev. Lett. **93**, 171104 (2004).
- [30] E. J. Copeland, M. Sami, S. Tsujikawa, Int. J. Mod. Phys. D **15**, 1753 (2006).
- [31] J. Yoo, Y. Watanabe, Int. J. Mod. Phys. D **21**, 1230002 (2012).
- [32] S. Hellerman, N. Kaloper, L. Susskind, JHEP **06**, 003 (2001).
- [33] T. Chiba, Phys. Rev. D **60**, 083508 (1999).
- [34] V. V. Kiselev, Class. Quantum Grav. **20**, 1187 (2003).
- [35] S. Chen, J. Jing, Class. Quantum Grav. **22**, 4651 (2005).
- [36] Y. Zhang, Y. X. Gui, Class. Quantum Grav. **23**, 6141 (2006).
- [37] S. Chen, B. Wang, R. Su, Phys. Rev. D **77**, 124011 (2008).
- [38] Y. H. Wei, Z. H. Chu, Chinese Phys. Lett. **28**, 100403 (2011).
- [39] B. B. Thomas, M. Saleh, T. C. Kofane, Gen. Relativ. Gravit. **44**, 2181 (2012).
- [40] S. Fernando, Mod. Phys. Lett. A **28** 1350189 (2013).
- [41] S. G. Ghosh, Eur. Phys. J. C **76**, 222 (2016).

- [42] Z. Xu, J. Wang, Phys. Rev. D **95**, 064015 (2017).
- [43] J. de Oliveira, R. D. B. Fontana, Phys. Rev. D **98**, 044005 (2018).
- [44] W. Xu, Y. Wu, EPL **121**, 40001 (2018).
- [45] K. Nozari, M. Hajebrahimi, S. Saghafi, Eur. Phys. J. C **80**, 1208 (2020).
- [46] K. Nozari, M. Hajebrahimi, Int. J. Geom. Methods Mod. Phys. **19**, 2250177 (2022).
- [47] R. Wang, F. Gao, H. Chen, Phys. Dark Universe **40**, 101189 (2023).
- [48] K. Ghaderi, B. Malakolkalami, Astrophys. Space Sci. **361**, 161 (2016).
- [49] M. S. Ma, R. Zhao, Y. Q. Ma, Gen. Relativ. Gravit. **49**, 79 (2017).
- [50] K. Ghaderi, B. Malakolkalami, Grav. Cosmol. **24**, 61 (2018).
- [51] Md. Shahjalal, Nucl. Phys. B **940**, 63 (2019).
- [52] F. Liu, L. C. Zhang, Chinese J. Phys. **57**, 53 (2019).
- [53] A. Haldar, R. Biswas, Gen. Relativ. Gravit. **52**, 19 (2020).
- [54] B. C. Lütfüoğlu, B. Hamil, L. Dahbi, Eur. Phys. J. Plus **136**, 976 (2021).
- [55] R. Ndongmo, S. Mahamat, T. Bouetou Bouetou, T. Crepin Kofane, Phys. Scr. **96**, 095001 (2021).
- [56] H. Chen, B. C. Lütfüoğlu, H. Hassanabadi, Z. -W. Long, Phys. Lett. B **827**, 136994 (2022).
- [57] B. Hamil, B. C. Lütfüoğlu, Eur. Phys. J. Plus **137**, 1124 (2022).
- [58] Y. Zhang, Y. B. Ma, Y. Z. Du, H. F. Li, L. C. Zhang, Eur. Phys. J. C **82**, 770 (2022).
- [59] B. Hamil, B. C. Lütfüoğlu, Nucl. Phys. B **990**, 116191 (2023).
- [60] B. Hamil, B. C. Lütfüoğlu, Phys. Dark Universe **42**, 101293 (2023).
- [61] W. H. Press, ApJ **170**, L105 (1971).
- [62] R. A. Konoplya, Gen. Relativ. Gravit. **34**, 329 (2002).
- [63] R. A. Konoplya, A. Zhidenko, Rev. Mod. Phys. **83**, 793 (2011).
- [64] B. P. Abbott et al. [LIGO Scientific and Virgo Collaborations], Phys. Rev. Lett. **116**, 061102 (2016).
- [65] B. P. Abbott et al. [LIGO Scientific and Virgo Collaborations], Phys. Rev. Lett. **119**, 161101 (2017).
- [66] R. A. Konoplya, Z. Stuchlik, A. Zhidenko, Phys. Rev. D **98**, 104033 (2018).
- [67] Á. Rincón, G. Panotopoulos, Phys. Rev. D **97**, 024027 (2018).
- [68] C. Chirenti, Braz. J. Phys. **48**, 102 (2018).
- [69] O. J. Tattersall, Phys. Rev. D **98**, 104013 (2018).

- [70] Y. S. Myung, D. -C. Zou, Phys. Lett. B **790**, 400 (2019).
- [71] R. A. Konoplya, A. F. Zinhailo, Z. Stuchlík, Phys. Rev. D **99**, 124042 (2019).
- [72] J. L. Blázquez-Salcedo, S. Kahlen, J. Kunz, Eur. Phys. J. C **79**, 1021 (2019).
- [73] R. A. Konoplya, A. F. Zinhailo, Eur. Phys. J. C **80**, 1049 (2020).
- [74] C. Liu, T. Zhu, Q. Wu, K. Jusufi et al, Phys. Rev. D **101**, 084001 (2020).
- [75] K. Jusufi, Phys. Rev. D **101**, 084055 (2020).
- [76] R. A. Konoplya, Phys. Lett. B **804**, 135363 (2020).
- [77] S. H. Hendi, A. Nemati, K. Lin, M. Jamil, Eur. Phys. J. C **80**, 296 (2020).
- [78] S. H. Hendi, S. Hajkhalili, M. Jamil, M. Momennia, Eur. Phys. J. C **81**, 1112 (2021).
- [79] S. Kanzi, I. Sakalli, Eur. Phys. J. C **81**, 501 (2021).
- [80] M. A. Anacleto, F. A. Brito, J. A. V. Campos, E. Passos, Ann. Phys. **434**, 168662 (2021).
- [81] I. Sakalli, G. Tokgöz Hyusein, Turk. J. Phys. **45**, 43 (2021).
- [82] K. Jafarzade, M. K. Zangeneh, F. S. N. Lobo, JCAP **04**, 008 (2021).
- [83] A. Ghosh, R. Brito, A. Buonanno, Phys. Rev. D **103**, 124041 (2021).
- [84] M. Okyay, A. Övgün, JCAP **01**, 009 (2022).
- [85] R. C. Pantig, L. Mastrototaro, G. Lambiase, A. Övgün, Eur. Phys. J. C **82**, 1155 (2022).
- [86] H. Chen, H. Hassanabadi, B. C. Lütfüoğlu, Z. W. Long, Gen. Relativ. Gravit. **54**, 143 (2022).
- [87] I. Sakalli, S. Kanzi, Turk. J. Phys. **46**, 1 (2022).
- [88] R. A. Konoplya, Phys. Rev. D **107**, 064039 (2023).
- [89] N. Heidari, H. Hassanabadi, Phys. Lett. B **839**, 137814 (2023).
- [90] M. A. Anacleto, F. A. Brito, J. A. V. Campos, E. Passos, Eur. Phys. J. C **83**, 298 (2023).
- [91] S. K. Jha, Eur. Phys. J. C **83**, 952 (2023).
- [92] G. Lambiase, R. C. Pantig, D. J. Gogoi, A. Övgün, Eur. Phys. J. C **83**, 679 (2023).
- [93] D. J. Gogoi, A. Övgün, D. Demir, Phys. Dark Universe **62**, 101314 (2023).
- [94] A. Al-Badawi, A. Kraishan, Chinese J. Phys. **87**, 59 (2024).
- [95] A. Das, A. R. Chowdhury, S. Gangopadhyay, Class. Quantum Grav. **41**, 015018 (2024).
- [96] K. Akiyama et al Event Horizon Telescope Collaboration et al, Astrophys. J. Lett. **875**, L1 (2019).
- [97] K. Akiyama et al Event Horizon Telescope Collaboration et al Astrophys. J. Lett. **930**, L12 (2022).
- [98] P. Z. He, Q. Q. Fan, H. R. Zhang, J. B. Deng, Eur. Phys. J. **80**, 1195 (2020).

- [99] V. Perlick, O. Y. Tsupko, Phys. Rep. **947**, 1 (2022).
- [100] J. L. Synge, Mod. Not. R. Astron. Soc. **131**, 463 (1966).
- [101] J. P. Luminet, Astron. Astrophys. **75**, 228 (1979).
- [102] J. M. Bardeen, in *Black Holes*, ed. by C. Dewitt, B. S. Dewitt (Gordon and Breach, New York), 215-239 (1973).
- [103] N. Tsukamoto, Z. Li, C. Bambi, JCAP **06**, 043 (2014).
- [104] N. Tsukamoto, Phys. Rev. D **97**, 064021 (2018).
- [105] R. Shaikh, Phys. Rev. D **100**, 024028 (2019).
- [106] R. A. Konoplya, Phys. Lett. B **795**, 1 (2019).
- [107] S. W. Wei, Y. C. Zou, Y. X. Liu, R. B. Mann, JCAP **08**, 030 (2019).
- [108] C. Bambi, K. Freese, S. Vagnozzi, L. Visinelli, Phys. Rev. D **100**, 044057 (2019).
- [109] S. Vagnozzi, L. Visinelli, Phys. Rev. D **100**, 024020 (2019).
- [110] A. Allahyari, M. Khodadi, S. Vagnozzi, D. F. Mota, JCAP **02**, 003 (2020).
- [111] M. Khodadi, A. Allahyari, S. Vagnozzi, D. F. Mota, JCAP **09**, 026 (2020).
- [112] G. Z. Babar, A. Z. Babar, F. Atamurotov, Eur. Phys. J. C **80**, 761 (2020).
- [113] R. Kumar, S. G. Ghosh, Astrophys. J. **892**, 78 (2020).
- [114] M. Zhang, M. Guo, Eur. Phys. J. C **80**, 790 (2020).
- [115] P. C. Li, M. Guo, B. Chen, Phys. Rev. D **101**, 084041 (2020).
- [116] M. Ghasemi-Nodehi, M. Azreg-Aïnou, K. Jusufi, M. Jamil, Phys. Rev. D **102**, 104032 (2020).
- [117] F. Atamuratov, K. Jusufi, M. Jamil, A. Abdujabbarov, M. Azreg-Ainou, Phys. Rev. D **104**, 064053 (2021).
- [118] M. Zhang, J. Jiang, Phys. Rev. D **103**, 025005 (2021).
- [119] T. Bronzwaer, H. Falcke, Astrophys. J. **920**, 155 (2021).
- [120] J. Peng, M. Guo, X. H. Feng, Chinese Phys. C **45**, 085103 (2021).
- [121] A. Chowdhuri, A. Bhattacharyya, Phys. Rev. D **104**, 064039 (2021).
- [122] J. Rayimbaev, B. Majeed, M. Jamil, K. Jusufi, A. Wang, Phys. Dark Universe **35**, 100930 (2022).
- [123] B. P. Singh, Ann. Phys. **441**, 168892 (2022).
- [124] R. Roy, S. Vagnozzi, L. Visinelli, Phys. Rev. D **105**, 083002 (2022).
- [125] Y. Chen, R. Roy, S. Vagnozzi, L. Visinelli, Phys. Rev. D **106**, 043021 (2022).
- [126] R. C. Pantig, L. Mastrototaro, G. Lambiase, A. Övgün, Eur. Phys. J. C **82**, 1155 (2022).

- [127] K. S. Virbhadra, Phys. Rev. D **106**, 064038 (2022).
- [128] S. L. Adler, K. S. Virbhadra, Gen. Relativ. Gravit. **54**, 93 (2022).
- [129] Y. -Z. Du, H. -F. Li, X. -N Zhou, W. -Q. Guo, R. Zhao, Chinese Phys. C **46**, 122002 (2022).
- [130] A. Das, A. Saha, S. Gangopadhyay, Class. Quantum Grav. **40**, 015008 (2023).
- [131] W. D. Guo, S. W. Wei, Y. X. Liu, Eur. Phys. J. C **83**, 197 (2023).
- [132] A. Uniyal, S. Kanzi, I. Sakalli, Eur. Phys. J. C **83**, 668 (2023).
- [133] A. Övgün, R. C. Pantig , A. Rincón, Eur. Phys. J. Plus **138**, 192 (2023).
- [134] N. U. Molla, U. Debnath, Ann. Phys. **453**, 169304 (2023).
- [135] G. J. Olmo, J. L. Rosa, D. Rubiera-Garcia, D. Sáez-Chillón Gómez, Class. Quantum Grav. **40**, 174002 (2023).
- [136] B. Hamil, B. C. Lütfüoğlu, L. Dahbi, arXiv:2307.16287 [gr-qc].
- [137] D. P. Theodosopoulos, T. Karakasis, G. Koutsoumbas, E. Papantonopoulos, arXiv:2311.02740 [gr-qc].
- [138] F. Atamuratov, M. Jamil, K. Jusufi, Chinese Phys. C **47**, 035106 (2023).
- [139] B. Hamil, B. C. Lütfüoğlu, Chinese Phys. C **48**, 055102 (2024).
- [140] H. Hoshimov, O. Yunusov, F. Atamurotov, M. Jamil, A. Abdujabbarov, Phys. Dark Universe **43**, 101392 (2024).
- [141] H. S. Snyder, Phys. Rev. **71**, 38 (1947).
- [142] P. Nicolini, Int. J. Mod. Phys A **24**, 1229 (2009).
- [143] P. Nicolini, J. Phys. A: Math. Gen. **38**, L631 (2005).
- [144] F. Nasser, Gen. Relativ. Gravit. **37**, 2223 (2005).
- [145] P. Nicolini, A. Smailagic, E. Spallucci, Phys. Lett. B **632**, 547 (2006).
- [146] T. G. Rizzo, JHEP **09**, 021 (2006).
- [147] Y. S. Myung, Y. -W. Kim, Y. -J. Park, JHEP **02**, 012 (2007).
- [148] B. P. Dolan, K. S. Gupta, A. Stern, Class. Quantum Grav. **24**, 1647 (2007).
- [149] K. Nozari, b. Fazipour, Mod. Phys. Lett. A **22**, 2917 (2007),
- [150] W. Kim, E. J. Son, M. Yoon, JHEP **04**, 042 (2008).
- [151] R. Banerjee, B. R. Majhi, S. Samanta, Phys. Rev. D **77**, 124035 (2008).
- [152] K. Nozari, S. H. Mehdipour, Class. Quantum Grav. **25**, 175015 (2008).
- [153] I. Arraut, D. Batic, M. Nowakowski, Class. Quantum Grav. **26**, 245006 (2009).
- [154] P. Nicolini, E. Spallucci, Class. Quantum Grav. **27**, 015010 (2010).

- [155] S. H. Mehdipour, Commun. Theor. Phys. **54**, 845 (2010).
- [156] M. Sharif, W. Javed, Can. J. Phys. **89**, 1027 (2011).
- [157] F. Rahaman, P. K. F. Kuhfittig, B. C. Bhui, M. Rahaman, S. Ray, U. F. Mondal, Phys. Rev. D **87**, 084014 (2013).
- [158] M. A. Anacleto, F. A. Brito, J. A. V. Campos, E. Passos, Phys. Lett. B **737**, 6 (2014).
- [159] M. A. Anacleto, F. A. Brito, E. Passos, Phys. Lett. B **743**, 184 (2015).
- [160] Y. G. Miao, Z. M. Xu, JCAP **03**, 046 (2017).
- [161] M. A. Anacleto, F. A. Brito, A. G. Cavalcanti, E. Passos, J. Spinelly, Gen. Relativ. Gravit. **50**, 23 (2018).
- [162] C. A. Soto-Campos, S. Valdez-Alvarado, Can. J. Phys. **96**, 1259 (2018).
- [163] M. A. Anacleto, F. A. Brito, E. Passos, Phys. Lett. B **803**, 135334 (2020).
- [164] M. A. Anacleto, F. A. Brito, S. S. Cruz, E. Passos, Int. J. Mod. Phys. A **36**, 2150028 (2021).
- [165] M. A. Anacleto, F. A. Brito, B. R. Carvalho, E. Passos, Adv. High Energy Phys. **2021**, 6633684 (2021).
- [166] A. Crespo-Hernandez, E. A. Mena-Barboza, M. Sabido, Int. J. Mod. Phys. D **31**, 2250127 (2022).
- [167] T. Juric, F. Pozar, Symmetry **15**, 417 (2023).
- [168] A. T. N. Silva, M. A. Anacleto, L. Casarini, arxiv: 2310.08852 [gr-qc].
- [169] J. Liang, Chinese Phys. Lett. **35**, 010401 (2018).
- [170] J. Liang, Chinese Phys. Lett. **35**, 050401 (2018).
- [171] Z. Yan, C. Wu, W. Guo, Nucl. Phys. B **961**, 115217 (2020).
- [172] Y. Zhao, Y. Cai, S. Das, G. Lambiase, E. N. Saridakis, E. C. Vagenas, arXiv: 2301.09147 [gr-qc].
- [173] J. A. V. Campos, M. A. Anacleto, F. A. Brito, E. Passos, Sci. Rep. **12**, 8516 (2022).
- [174] P. R. Giri, Int. J. Mod. Phys. A **22**, 2047 (2007).
- [175] M. Jamil, F. Rahaman, R. Myrzakulov, P. Kuhfittig, N. Ahmed, U. Mondal, J. Korean Phys. Soc. **65**, 925 (2014).
- [176] F. Rahaman, A. Banerjee, M. Jamil, A. K. Yadav, H. Idris, Int. J. Theo. Phys. **53**, 1919 (2014).
- [177] I. Arraut, D. Batic and M Nowakowski, Class. Quantum Grav. **26**, 245006 (2009).
- [178] M. Saleh, B. T. Bouetou and T. C. Kofane, Astrophys. Space Sci. **333**, 449 (2011).
- [179] B. P. Singh, Ann. Phys. **441**, 168892 (2022).
- [180] S. Hui, B. Mu and P. Wang, Phys. Dark Universe **43**, 101396 (2024).
- [181] K. Ghaderi and B. Malakolkalami, Nuc. Phys. B **903**, 10 (2016).

- [182] T. Toghray, A. El Boukili, N. Mansour, H. Lekbich, A. K. Daoudia and M. B. Sedra, *Ind. J. Phys.* **97**, 4497 (2023).
- [183] A. Rogers, *Mon. Not. R. Astron. Soc.* **451**, 4536 (2015).
- [184] A. Abdujabbarov, B. Toshmatov, Z. Stuchlík, B. Ahmedov, *Int. J. Mod. Phys. D* **26**, 1750051 (2016).
- [185] U. Papnoi, F. Atamurotov, S. G. Ghosh, B. Ahmedov, *Phys. Rev. D* **90**, 024073 (2014).
- [186] N. Herceg, T. Jurić, A. Samsarov, I. Smolić, arxiv:2310.06038 [hep-th].
- [187] N. Herceg, T. Jurić, A. Samsarov, I. Smolić, K. S. Gupta, arxiv:2310.06018 [hep-th].
- [188] R. Moderski, M. Rogatko, *Phys. Rev. D* **64**, 044024 (2001).
- [189] H. T. Cho, *Phys. Rev. D* **68**, 024003 (2003).
- [190] J. Jing, *Phys. Rev. D* **69**, 084009 (2004).
- [191] C. -Y. Chen, P. Chen, *Phys. Rev. D* **99**, 104003 (2019).
- [192] M. Bouhmadi-Lopez, S. Brahma, C. -Y. Chen, P. Chen, D. Yeom, *J. Cosmol. Astropart. Phys.* **07**, 066 (2020).
- [193] B. F. Schutz, C. M. Will, *Astrophys. J. Lett.* **291**, 184453 (1985).
- [194] S. Iyer, C. M. Will, *Phys. Rev. D* **35**, 3621 (1987).
- [195] R. Konoplya, A. Zhidenko, A. Zinhailo, *Class. Quant. Grav.* **36**, 155002 (2019).
- [196] J. Matyjasek, M. Opala, *Phys. Rev. D* **96**, 024011 (2017).
- [197] B. Mashhoon, *Phys. Rev. D* **31**, 290 (1985).
- [198] V. Ferrari, B. Mashhoon, *Phys. Rev. D* **30**, 295 (1984).